The landscape of cancer rewired GPCR signaling axes.

Chakit Arora[1], Marin Matic[1], Pierluigi DiChiaro[2], Natalia De Oliveira Rosa[1], Lauren Clubb[3], Lorenzo Nemati[1], Giorgos Kargas[1], Ranka Vukotic[4], Luana Licata[5], Guanming Wu[6], Giuseppe Diaferia[2], Gioacchino Natoli[2], J. Silvio Gutkind[3] and Francesco Raimondi[1+]

1 Laboratorio di Biologia Bio@SNS, Scuola Normale Superiore, Piazza dei Cavalieri 7, 56126, Pisa, Italy; 2 2 Department of Experimental Oncology, IEO, European Institute of Oncology IRCCS, Milano, Italy; 3 Department of Pharmacology and Moores Cancer Center, University of California, San Diego, La Jolla, CA 92093, USA; 4 Azienda Ospedaliero-Universitaria Pisana, Via Roma, 67, 56126 Pisa; 5 Department of Biology, University of Rome 'Tor Vergata', Rome 00133, Italy; 6 Division of Bioinformatics and Computational Biology, Department of Medical Informatics and Clinical Epidemiology, Oregon Health & Science University, Portland, Oregon, USA.

+ To whom correspondence should be addressed: francesco.raimondi@sns.it

Abstract

We explored the dysregulation of GPCR ligand signaling systems in cancer transcriptomics datasets to uncover new therapeutics opportunities in oncology. We derived a network of interacting ligands and biosynthetic enzymes of organic ligands to infer extracellular activation processes, which we combined with cognate GPCRs and downstream effectors to predict GPCR signaling pathway activation. We found multiple GPCRs that are differentially regulated together with their ligands across cancers and revealed a widespread perturbation of these signaling axes in specific cancer molecular subtypes. We showed that biosynthetic pathway enrichment from enzyme expression recapitulated pathway activity signatures from metabolomics datasets, therefore providing valuable surrogate information for GPCRs responding to organic ligand systems. The expression of several GPCRs signaling components was significantly associated with patient survival in a cancer subtype specific fashion. In particular, the expression of both receptor-ligand, as well as receptor-biosynthetic enzymes interaction partners improved the stratification of patients based on survival, suggesting a potential synergistic role for the activation of specific GPCR networks in modulating cancer phenotypes. Remarkably, we identified many receptor-ligand or enzyme

pairs to be significantly associated with patient survival across several cancer molecular subtypes. Furthermore, we found that GPCRs from these actionable axes are the targets of multiple drugs displaying anti-growth effects in large, drug repurposing screens in cancer cells. This study provides a comprehensive map of GPCR signaling axes that can be exploited as actionable targets for personalized cancer treatments. We have made the results generated in this study freely available for further exploration to the community through a webapp (gpcrcanceraxes.bioinfolab.sns.it).

Introduction

G-protein coupled receptors (GPCRs) are the largest family of transmembrane proteins which transduce a wide number of physical and chemical stimuli into the cell by coupling to intracellular heterotrimeric G-proteins, thereby controlling multiple downstream signaling pathways and transcriptional programs[1–3]. The GPCRs repertoire expanded and diversified to meet the increasing need for inter-cellular communication in evolving multicellular organisms[4,5]. Systematic efforts are being undertaken to illuminate the complex circuitry of GPCR signaling both at the intracellular [5–10] as well as the extracellular ligand level[11].

Cancer genomics provides the possibility to systematically shed light on cancer somatic alterations affecting GPCRs as well as their interacting partners [12–16]. The GPCR-based circuitry is frequently disarranged in cancer. Indeed, a landscape of GPCR-centric autocrine, paracrine, juxtacrine or endocrine signaling networks is emerging as a critical component for the interaction of cancer cells with their tumor micro-environment (TME), ultimately leading to cancer progression and therapy resistance[14,15]. For instance, chemokines, such as *CXCL1*, *CXCL2*, and *CXCL8,* bind and activate their receptors, primarily *CXCR1* and *CXCR2* on immune suppressive myeloid derived cells thereby disabling anti-tumoral immune surveillance mechanisms[14]. Several GPCRs and their associated components mediating inflammation have also been connected to immune evasive TME, such as prostaglandins (in particular *PGE2*), their biosynthesizing enzymes (*PTGS1* and *PTGS2*) and cognate prostanoid receptors (e.g., *PTGER2* and *PTGER4*). Ectonucleotidases (such as *NT5E* or *ENTPD1*) and adenosine receptors are also well known to induce an immunosuppressive tumor microenvironment[14]. Recent studies have also shown the emergent role of innervation in promoting tumor growth (reviewed in[17]). Notably, it has emerged a cross-talk between the neurotrophin pathway, particularly the *NGF-NTRK1* axes, and GPCR signaling mediated by either (nora)adrenaline-*ADRB2* in pancreatic cancer[18], or acetylcholine-*CHRM1 and CHRM3*

in gastric cancer[19]. However, defining these immune evasive and tumor promoting networks has been elusive.

In this regard, single cell and spatial sequencing technologies are allowing us to study mechanisms of cell-cell communications at an unprecedented resolution[20]. In the most comprehensive resource to date used to infer ligand-receptor pairs mediating cell-cell communication[21], GPCRs-ligand interactions are surprisingly depleted, representing roughly less than 5% of the total curated interactions, despite being the most abundant class of transmembrane proteins involved in signal transmission. This is likely due to the fact that many GPCRs bind to small organic molecules, including neurotransmitters and multiple metabolites, which cannot be detected via transcriptomics techniques.

In the present study, we considered an extended network of signaling axes formed by GPCRs with interacting ligands, as well as biosynthetic enzyme pathways, to systematically explore their aberrant regulation in cancer transcriptomics datasets and investigate their prognostic value for personalized medicine treatments.

Results

GPCRs extracellular signaling system

We first generated a comprehensive catalog of upstream and downstream molecular interactions involving GPCRs (Figure1a-c; see Methods). Briefly, we retrieved known GPCR ligands from IUPHAR/Guide to Pharmacology database (GtoPDB), which we mapped to individual ligand-synthesizing enzymes as well as to known biosynthetic pathways, and to pathways mediating signal transduction (Methods; Table S1,2). This yielded a total of 236 ligands, 309 biosynthetic pathways and 82 enzymes associated instances (Figure 1a-c). We found that (86%) of ligands and (99%) of enzymes were already annotated within biological pathway knowledgebases (i.e., Reactome; Figure 1b). A total of 211 (53%) non-olfactory receptors have known ligands in GtoPdb, 95 of which exclusively bind organic ligands, 90 peptides and 26 both ligand types (Figure 1b). While the vast majority of peptide ligands are annotated to participate in signaling pathways, the organic ligands are instead extensively annotated as part of metabolic processes (Figure 1b; Table S1).

We then computed genome-wide differential expression (DE) by contrasting cancer samples from the TCGA to those from corresponding healthy tissues from GTEx to derive expression signatures of genes and pathways mediating GPCR signaling. We considered a total of

15000 samples, of which 10500 were from TCGA and 4500 from GTEX, encompassing 16 tissues, as well as 79 cancer molecular subtypes (see Methods; Table S3).

Remarkably, we found a widespread, cancer-specific regulation of GPCR-related genes with respect to healthy tissues. We found on average 91 up-regulated and 92 down-regulated GPCRs (FDR < 0.01, |log2FC|>1) across cancer tissues. When considered together with their cognate ligands and biosynthetic enzymes, we obtained an average of 161 up-regulated and 133 down-regulated instances (Figure 1d). The amount of significantly DE genes varies across tissues, with Testis, Skin and Ovary being the most affected, and Bladder the least (Figure 1d). Certain cancer tissues are characterized by a prevalence of either significantly over-expressed (e.g., Pancreas) or downregulated (e.g., Brain) GPCRs (Figure S1a). We found no significant trend when grouping DE receptors based on their G-protein coupling specificity (Figure S1a). On the other hand, DE profiling of heterotrimeric G-protein α subunits showed that *GNAS* is the single subunit most widely up-regulated, being significantly over-expressed in 94% of cancer tissues (Figure S1b,c), confirming previous analyses[14,16].

At the process level, we found a widespread DE regulation (FDR < 0.01) of GPCR pathways across cancers (Figure 1e). In particular, 40% of cancer tissues are either more enriched in biosynthetic or signal transduction processes, while 20% of cancer tissues are equally affected in both (Figure 1e). Several pathways are found to be widespread affected (e.g., up-regulation of Chemokine receptors), while others are exclusively regulated in certain tumor types (Figure S1d). Overall, these data show that every cancer tissue is characterized by a highly specific GPCR pathway signatures (Figure S1d).

The landscape of peptide ligand-GPCRs dysregulation in cancer

We focused our analysis on the extracellular components of the GPCR signaling machinery, e.g., ligands and related metabolizing enzymes, to understand their contribution to the overall dysregulation of GPCR signaling in cancer.

We found on average 66 significantly DE peptide ligand precursors in 16 cancer tissues, and on average 60 instances in 79 molecular subtypes.

We next assessed the degree of correlation of expression change between receptors and interacting ligands and found a widespread co-regulation of receptor-ligand precursor pairs in multiple cancer tissues and subtypes (Figure 2a, Figure S2; see Methods). By focusing on the receptor-ligand pairs more recurrently co-regulated, we identified two clusters, showing respectively a prevalence of concordantly up-regulated (i.e., Cluster 1) and concordantly

down-regulated (i.e., Cluster 2) axes across subtypes (Figure 2a). The vast majority of the most frequently regulated ligands are agonists, with the exception of *CCL4*, *CCL7* and *CXCL8,10,11*, which might act as either agonists or antagonists depending on the bound receptor (Figure 2a). Most of axes in Cluster 1 involve chemokine receptors (e.g., *CCR1, CCR3, CCR4, CCR5, CCR6, CCR8, CXCR3, CXCR6, XCR1*) as well as other receptors such as *APLNR*, *CALCR*, *GRPR, MCHR1, GPR37, CCKBR, NPBWR1, KISS1R* and their cognate ligands. The main transduction mechanism in this group is through $G_{i/o}$ proteins, as well as to a lesser extent via $G_{q/11}$ and $G_{12/13}$ (Figure 2a).

Cluster 2 contains instead receptor-ligand axes that are more frequently concordantly down-regulated in cancer subtypes, although several of these are concordantly up-regulated in other specific subtypes (e.g., *CXCR2, EDNRB, FFPR2*, or *LGR6, GALR2* and *UTS2R;* Figure 2a). The axes in Cluster 2 involve receptors that are members of various families from class A and B. Receptors in this group have a more heterogeneous/promiscuous coupling profile to $G_{q/11}$, $G_{i/o}$ and G_s, but very little to $G_{12/13}$ (Figure 2a).

In general, every cancer subtype is characterized by a highly specific receptor-ligand co-expression signature. However, certain tissues display similar subtype co-expression patterns (e.g., liver, breast, ovary, thyroid, stomach, lung, skin and pancreas). Others show higher heterogeneity (e.g., kidney, colon, bladder, esophagus, prostate, brain) (Figure 2a).
Co-regulation patterns of a given receptor can vary, depending on the tissue as well on the number and type of bound ligands (Figure 2b, Figure S2). Certain receptors display consistent co-regulation patterns across cancer tissues and subtypes even if bound to multiple ligands (e.g., *CXCR3, CCR3*, *CCR5*; Figure 2b,2c). Others show more variable co-regulation patterns which vary in a tissue (or subtype) and ligand specific fashion (e.g., *CALCRL* or *RXFP2*; Figure 2b,c).

Expression of biosynthetic pathway enzymes inform on the levels of organic endogenous ligands

We reasoned that the expression levels of the enzymes synthesizing organic GPCR ligands could be informative of their levels and thus be used as a proxy to model ligand abundance in transcriptomic datasets that miss this kind of information. To this end, we assessed enzyme and biosynthetic pathway activities from differential expression signatures (see Methods).

We found on average 63 and 8 significantly regulated enzymes and biosynthetic pathways, respectively, across cancers, suggesting a widespread dysregulation of GPCR ligand biosynthetic pathways in human malignancies, which in some cases were specific to distinct cancer subtypes (Figure 3a). Clustering of biosynthetic pathways based on enrichment scores revealed two main clusters: one characterized by processes, such as those related to selenocysteine synthesis and di/triphosphate nucleotide interconversion, which are overall up-regulated in most cancer subtypes, while the others are characterized by processes recurrently down-regulated, such as “Phase I - Functionalization of compounds” or “Eicosanoids” (Figure 3a). Other biosynthetic pathways are specifically enriched in given cancer subtypes. For example, “Arachidonic acid metabolism” is down-regulated in several Kidney and Skin cancer subtypes, while it is significantly up-regulated in Ovary “Mesenchymal” and Glandular “GL” Pancreas subtypes. Other pancreatic cancer subtypes, such as the Transitional (“TR”) and Undifferentiated (“UN”), displayed instead significant enrichment of “Synthesis of Prostaglandins (PG) and Thromboxanes (TX)” pathway (Figure 3a).

In order to determine if DE gene transcripts are mirrored by differential expression of the corresponding metabolites, we compared pathway enrichment scores of DE transcripts with differential abundance scores of DE metabolites from a pancancer metabolomic profiling dataset[22], considering a set of curated biosynthetic pathways (e.g., Reactome; see Methods;Table S4). We found a total of 33 significant pathways (FDR < 0.01) in at least one of the 5 cancer types considered, and which showed concordant pathway enrichment when considering both differentially expressed transcripts and metabolites (Figure 3b). The cancer type showing the highest number of concordant signatures is pancreatic adenocarcinoma (PAAD). Certain pathways show concordant up-regulation in multiple cancer types, including: “activation of gene expression by SREBF (SREBP)”, “Purine catabolism”, “Pyruvate metabolism”, each found up-regulated in three distinct cancer types (Figure 3b). For example, “Purine catabolism” is always up-regulated when considering both transcriptome and metabolome in Breast, Pancreas and Prostate cancers (Figure 3c). Inspection of differentially expressed genes and metabolites on a functional interaction network shows that over-activation of the pathway is contributed by over-expression of both transcripts and metabolites components (Figure 3e). However, only a few enzymes or metabolites in this pathway are invariably over-expressed across cancers (e.g., *NUDT1*, *LEF1*, 9H-Xanthine; Figure 3d, Figure S3). Other processes show concordant enrichment with a cancer dependent directionality: e.g., nicotinate metabolism, which is up-regulated in pancreas and down-regulated in prostate, or creatine metabolism, down-regulated in pancreas and up-regulated in breast (Figure 3b). Several other pathways are exclusively

enriched in specific cancer tissues: for example, “Glucagon-like Peptide-1 (GLP1) regulates insulin secretion”, “Synthesis of Prostaglandins (PG) and Thromboxanes (TX)” and “Acetylcholine regulates insulin secretion” are hallmarks of pancreatic cancer and might contribute to reinforce the known role of the Gs-PKA signaling axis in this cancer type [23,24].

Expression of GPCRs signaling network components correlates with patient survival

We systematically assessed correlations between expression of GPCR network components and patient survival. Briefly, we defined groups of patients based on the expression of a GPCR component, i.e., high or low expression, respectively, if above or below the median of the distribution of expression values of that gene in the samples and tested whether these groups had significantly different survivals (see Methods).

We first considered the capability of the expression of individual components (e.g., receptors, transducers, ligand or biosynthetic enzymes) to discriminate patients based on their survival. We found a total of 302 unique significant receptor instances (LogRank P-value < 0.05, FDR < 0.1) in 11 cancer tissues, 103 ligands in 10 cancers, and 71 enzymes in 10 cancers (Figure 4a; Table S5-7). Some cancer tissues display overall more components whose expression is associated with either higher (e.g., pancreas, skin or head and neck) or lower (e.g., brain, breast, lining of body cavities and white blood cell) survival (Figure 4a). Overall, the expression of GPCR genes is associated with poorer survival in the 59% of cases across all cancers. *CELSR3*, *GPR25, EDNRB and F2RL2* are significantly associated with patients’ survival in four cancers each, with an equal prevalence for lower and higher survival (Figure 4b, Table S5). Some receptors show consistent associations across cancers: for example, *ADORA2A* is invariably associated to higher survival across four distinct cancer tissues (including pancreas, breast, skin and head and neck; Figure 4b), which might be consistent with its known role in regulating CD8+ T cell activity and survival in the tumor microenvironment[25]. Certain receptors are instead invariably associated with poorer survival, such as *OXTR, ADORA2B, GPR3, FZD6, GPRC5A and LPAR3*. We also found a large prevalence of associations between GPCR peptide ligand precursor expression and lower survival of patients, with 67.2% of the significant instances across cancers. Among the most recurring ligands, we found several instances that are either invariably associated to lower survival, e.g., *CXCL5*, *CXCL1, GAL* and *RPS19*, or have opposite associations depending on the cancer type, e.g., *CXCL9, C3, CCL26, CCL8, CCL13, RSPO1, RLN1, RLN2* and *UCN* (Figure 4b; Table S6).

We reasoned that in those patients with higher expression of both receptors and ligands (or biosynthetic enzymes), a likely enhanced activation of the signaling axis should better

correlate with specific patient phenotypes (e.g., lower or higher survival) than when considering individual components. We therefore assessed differences in the survival of patients grouped on the basis of the expression levels of GPCRs and ligand precursors (or enzymes) either alone or in combination. We then shortlisted receptor ligand pairs characterized by higher significance as well as greater hazard ratios of patient survival compared to the individual interaction partners (Figure 4c; Table S8-9, see Methods). Intriguingly, we found several axes, such as *NPBWR2-NPW, PRHLR-NPY, PRLHR-PLR, CRHR2-UCN3, CALCR-CALCB,* associated with lower survival more significantly than considering interaction partners alone in multiple cancer types (Figure 4c,d; Figure S4). Certain cancer types show multiple significant instances of associations between receptor-ligand axis and survival (e.g., lower survival in adrenal gland, eye; Figure 4c), suggesting a potential polypharmacology strategy for these tumor types.

Interestingly, it appears that some receptors participating in significant axes within the same cancer type share, to some extent, similar signal transduction mechanisms, suggesting that the patient survival phenotype might be contributed by multiple ligand stimuli converging on common signaling cascades. For example, in head and neck cancers we found significant correlation of higher survival and higher expression of *SSTR2-SST* (Figure S5a*), RXFP3-INSL5* and *RXFP1-RLN3* signaling axis, which all share similar coupling profiles (e.g., $G_{q/11}$, particularly *GNA14*, as well as $G_{i/o}$; Figure S6). *RXFP1-RLN3* is instead associated with lower survival in breast carcinoma patients, highlighting the specificity of survival associations of these axes with cancer subtypes. Likewise, *SSTR2-SST* is associated to lower survival in Adrenal Gland patients (Figure S5b), *OPRK1-POMC* with lower survival in uveal melanoma and higher survival in Lining of body cavities, *CXCR2-CXCL6* with lower survival in Adrenal Gland and higher survival in Lining of body cavities, *TACR2-TAC1* is associated with lower survival in Liver cancer and higher survival in Cervix and Uterus.

Notably, some of the receptor-ligand pairs that we found differentially co-regulated in terms of expression, are also significantly associated with survival differences (Figure 4e). In details, we found a total of 24 receptor-ligand pairs from 15 cancer subtypes. *CCR5* is the receptor-ligand forming pair (with *CCL7* and *CCL8*) that is more frequently concordantly DE-regulated, being at the same time significantly associated with survival. In particular, *CCR5* concordant up-regulation is invariably associated with a better prognosis, irrespective of the cancer subtype considered. Other pairs, such as those mediated by *CXCR2,* display cancer subtype-specific patterns of both differential expression regulation and correlation with patient survival (Figure 4e). On the other hand, pairs such as *CCR1-CCL4* are always co-up regulated but with different prognostic values, i.e., they are associated to higher survival in

melanoma (RAS and BRAF hotspot mutants subtypes), and to lower survival in gastric cancer ("GI.GS" subtype, Figure 4e). The latter is also an example of cancer subtype with multiple axes association to lower survival. Other subtypes, such as the Glandular ("GL") Pancreas, are instead characterized by multiple axes associated to higher survival (Figure 4e). Overall, we found 124 receptor-ligand pairs in 48 cancer subtypes more significantly correlated to survival than their individual instances (Figure S7).

Biosynthetic enzymes and cognate GPCRs form surrogate signaling pairs with prognostic value.

We found multiple ligand-synthesizing enzymes whose expression correlates with patients' survival in multiple cancers, with 70% of them significantly linked to worse survival (LogRank P-value < 0.05, FDR<0.1). Remarkably, the 5'-nucleotidase *NT5E* is invariably associated to lower survival in four distinct cancer types, including breast, brain, stomach and pancreas (Figure 4b; Table S7). Other enzymes most recurrently associated with lower survival are Lysophosphatidylcholine acyltransferase 2 (*LPCAT2*), Beta-1,4-galactosyltransferase 3 (*B4GALT3),* as well as prostacyclin synthase (*PTGIS*). On the other hand, enzymes such as Bis(5'-adenosyl)-triphosphatase (*ENPP4)*, Arylsulfatase G (*ARSG)* and the Long-chain fatty acid transport protein 2 *(SLC27A2)* are recurrently associated to higher survival (Figure 4b).

Every time that the cognate ligand was a small organic molecule, we considered the corresponding synthesizing enzymes and we similarly checked for an improvement of the survival statistics when considering the combined expressions of interaction partners (Methods; Table S9). This revealed several instances involving biosynthetic enzymes for neurotransmitters and cognate receptors (Figure 5A, Table S9). Multiple pairs involve enzymes for monoamine neurotransmitter biosynthesis, such as Tryptophan 5-hydroxylase 2 (*TPH2*), the rate-limiting enzyme for serotonin synthesis, which is significantly associated to lower survival with multiple serotonergic receptors (e.g., *HTR1A* in Liver, *HTR2C* and *HTR6* in Adrenal Gland and *HTR7* in White Blood cell). Several Dopamine receptors are significantly correlated along with enzymes mediating catecholamine biosynthesis, including *DDR3-DDC* (liver), *DDR2* and *DDR3-TH* (prostate). The latter enzyme, which rate-limits the catecholamine pathway, is also significantly associated with *ADRA1D* in Lymphatic Tissue. The axis formed by Choline O-acetyltransferase (*CHAT)* and muscarinic receptors *CHRM1,3,5* are associated with lower survival in multiple cancers (Fig. 5a, b). The three axes involving muscarinic receptors and *CHAT* are all associated to lower survival in liver cancer, with *CHRM3-CHAT* being also significantly correlated in Esophageal cancer (Fig. 5a). We found multiple instances of glutamate receptors (e.g., *GRM1,2,4,5*) and Glutamate decarboxylase 1 and 2 (*GAD1,2*). While the *GRM2-GAD1* receptor-biosynthetic pathway pair

shows tissue specific correlation with survival, being associated with lower survival in Adrenal Gland and with higher survival in Liver, the axes of *GAD2* with *GRM1,4,5* are always significantly associated with lower survival in Endometrium and Thyroid cancer tissues. We also found several instances of receptors for purines whose aberrant expression co-occur with that of multiple enzymes of the Purine catabolism pathway. In details, while the *ADORA2B-PNP* pair is associated to lower survival in Uterus (Figure 5a,b), *P2RY4* axes with *ENPP3* and *ENTPD1* are associated to higher survival in the same cancer. The latter axis is instead significantly associated with lower survival in Adrenal Gland (Figure 5a). Overall, we found 115 receptor-enzyme pairs in 45 cancer subtypes more significantly correlated to survival than individual instances (Figure S8).

Drugs for GPCR networks hold the potential to inhibits cancer cell growth

We retrieved GPCRs ligands showing cancer growth inhibitory capacity from a public resource containing the growth-inhibitory activity of 4,518 drugs tested across 578 human cancer cell lines[26]. A total of 13 out of 52 GPCR ligands tested were found to significantly inhibit the growth of cancer cell lines (Figure 6a)[26]. We checked the targets of these ligands on the pooled list of GPCRs that we found to mediate axes significantly associated with cancer survival. Strikingly, all these drugs bind to receptors that are significantly coregulated axes with either their ligands or biosynthetic enzymes (Figure 6a,b; Table S10). In particular, among them we found multiple ligands targeting certain GPCRs classes, including adenosine receptors (i.e., CGS-15943, MRS-1220, SCH-58261), muscarinic receptors (i.e., VU0238429, xanomeline, terfenadine) and opioid receptors (i.e., BNTX and JTC-801). Interestingly, the vast majority (76%) of these drugs are antagonists. Moreover, receptors targeted by antagonists appear to be more promiscuous, and coupling primarily to $G_{q/11}$ or $G_{i/o}$, but also to a lesser extent to G_s and $G_{12/13}$ proteins (Figure 6c).

Discussion

In recent years the multifaceted role of GPCR signaling in cancer has begun to emerge[14,15], though an overall mechanistic picture is still lagging. At a molecular level, this is mainly due to the lack of a precise mechanistic understanding of how receptors transduce external signals intracellularly in the context of the TME, as well as how the upstream ligand and biosynthetic pathway components contribute to trigger an aberrant GPCR signaling network in tumor cells and their associated stroma and infiltrating immune cells. At a higher level, the complex circuitry wired by multi-component GPCRs systems is highly tailored to specific

cellular contexts. Pathways dysregulation might be initiated through perturbations of these multi-component systems at different levels, all of which may converge to an overall dysregulation and/or persistent activation of GPCR downstream signaling.
In the present study, we systematically inferred GPCR pathways activities from cancer transcriptomic datasets, with a special focus on the dysregulation of GPCR signaling axes involving the co-deregulation of the expression of their direct ligands as well as biosynthetic pathways controlling their ligand availability.

We found that multiple GPCRs are co-regulated together with their cognate ligands or biosynthetic enzymes, suggesting a coordinated effect on the signaling axis. Some of these are widespread co-regulated across cancers, others are affected in specific tumor contexts. These studies revealed some exciting emerging patterns, among them that chemokine receptors and their cognate chemokines are certainly the most co-regulated axes. The precise role in pro- or anti-tumor immunity played by these chemokine receptor networks is known to depend on the precise cellular and tumor subtype context[14,27]. For example, the known tumor-promoting *CXCR2* is found co-down regulated together with *CXCL2* in liver cancer ("iCluster2" subtype) and with *PPBP*, the precursor of *CXCL7*, in lung ("LUAD.3" subtype). Remarkably, in both cases, the co-down-regulation is associated with higher survival (Figure 4e). The co-up regulation of this axis is associated with lower survival in stomach cancer ("GI.GS" subtype) and with higher survival in pancreatic cancer ("GL" subtype), similarly to *CXCR2-CXCL3*. Other chemokine receptors, such as *CCR1, CCR3* or *CCR5*, are significantly co-up regulated across different cancer subtypes. While *CCR1-CCL4* has distinct correlation to survival depending on the cancer type considered, *CCR5-CCL7* or *CCR5-CCL8* co-up regulation is always associated with higher survival, suggesting a general anti-tumor immunity of these axes in the cancer subtypes considered (Figure 4e).

Interestingly, we also found a few non-chemokine receptors that are widespread co-up activated, such as *KISS1, NPBWR, MCHR1 or APLNR* which suggest the existence of signaling mechanisms other than chemokine sustaining the cell-cell interaction within the TME. Another notable example of highly context specific co-regulation of signaling axes is the one mediated by *CALCR* and its close paralogue, *CALCRL*, whose interaction with *ADM* is a critical factor determining relapse and drug resistance in Leukemia[28].

We found that many of the co-regulated signaling axes are also associated with patient survival. For example, in head and neck cancer we have found multiple signaling axes significantly associated to higher survival, such as *SSTR2-SST*, *RXFP3-INSL5* and *RXFP1-RLN3*. Intriguingly, all the three receptors show converging couplings towards $G_{q/11}$ and Gi/o

proteins. Notably, the *SSTR2-SST* has been significantly associated to higher survival rates in EBV-nasopharyngeal cancer, a class of head and neck cancer, and its targeting with a miniaturized peptide-drug conjugate (i.e., PEN-221) has been proposed to treat this type of tumor[29]. *SSTR2-SST* is also one of the axes with the strongest literature support to a role in cancer, along with several others including e.g., *MC1R-POMC*, *GHRHR-GHRH* (Figure S9; Table S11).

Along with the mRNA expression of peptide ligand precursors, we also considered the expression of synthesizing enzymes as a proxy to model upstream signals from small organic ligands. Indeed we found a significant correlation of patients' survival with expression of axes formed by receptors and biosynthetic enzyme pairs. Similarly to the receptor-ligand axes, we found receptor-enzymatic axes recurrently associated with survival in a cancer-type specific fashion. For example, we found multiple instances of muscarinic receptors and Choline O-acetyltransferase (*CHAT*) co-regulation with patient outcome. Cholinergic signaling has been established as a key factor mediating gastric cancer tumorigenesis via an NGF promoted feed-forward loop[19]. Intriguingly, the association between the expression of muscarinic receptors-*CHAT* axis with lower survival in hepatocellular carcinoma correlates with the known involvement of acetycholinesterase, which opposes *CHAT* function by degrading acetylcholine, and is associated to better prognosis in HCC[30]. Other biosynthetic enzyme axes that we have identified are also supported by additional lines of evidence from the literature (Figure S9d). The information about biosynthetic enzymes is indeed particularly important for receptor systems such as GPCRs, which frequently bind to organic ligands, and might represent a resource complementing existing knowledge-bases for receptor-ligand interactions used to characterize cell-cell communication from spatial transcriptomics datasets[21]. It will be critical in the future to dissect the precise cell context-specific role played by these GPCRs signaling axes by analyzing single cell as well as spatial transcriptomics RNAseq datasets, as we recently began exploring in the context of CD8-T cell function[31].

Taken together, we have found a few hundreds of receptor pairs with either ligands or enzymes to be significantly associated to survival in tens of cancer molecular subtypes, suggesting a host of actionable opportunities to modulate oncogenic phenotypes. Strikingly, all the GPCR drugs that have been reported to significantly hamper cancer cell line growth in a recent systematic screen[26], indeed target receptors of axes that we found significantly correlated with patient survival. In addition to directly hampering cancer growth, the targeting of GPCRs network is emerging as a promising therapeutic option in combination with immunotherapy[14]. For instance, adenosine signaling is an established factor which dampens

the immune response in inflamed tissues and targeting of either adenosine receptors (particularly *ADORA2A*), or adenosine synthetizing enzymes (*NT5E* and *ENTPD1*) are currently being evaluated in combination with cancer immunotherapies[32,33]. Moreover, the G_s-PKA axis has been recently identified as a key pathway dampening the anti-tumor CD8 T cell activity and resulting in Immune Checkpoint Blockade failure. This study suggests that additional G_sPCRs (e.g., EP_2, EP_4, β_1AR, and β_2AR), other than *ADORA2A*, could be targeted in combination with immunotherapy[31].

Ultimately, our data-driven approach, that integrates high-dimensional transcriptomics datasets and highly curated signaling networks, may enable the functional interpretation of GPCRs' dysregulation mechanisms and guide the development of novel pharmacological strategies and drug repurposing opportunities targeting GPCRs in cancer.

Methods

GPCR signaling network

To create an extended GPCR network, we have extracted the GPCR and ligand interactions from the IUPHAR/BPS Guide to PHARMACOLOGY database (IUPHAR database)[34]. We retained only endogenous ligands, thereby extracting 243 GPCRs and 328 ligands. Based on database classification, the considered ligands can be grouped into five groups: 211 peptides, 107 metabolites, 7 synthetic organic, 2 inorganic and 1 natural product. All the other annotations describing GPCRs and ligands were also pulled from the database. To further extend our network we added biosynthetic enzymes for GPCR endogenous ligands. To this end we used Rhea, a curated database of chemical reactions of biological relevance[35]. To identify metabolizing enzymes for GPCRs ligands, we first referenced IUPHAR ligands to ChEBI[36], which is used by Rhea to identify ligands. Ligand mapping between IUPHAR and Rhea was carried out by using the IUPHAR International Chemical Identifiers (InChIs). As many of the chemical reactions are happening under physiological pH of 7.3, the ChEBI identities of participants in Rhea reactions at pH 7.3 were considered. Using our in-house python scripts, we have extracted all the enzymes catalyzing reactions where GPCR ligands participate as products, meaning that most of the reactions have left-right (LR) directionality or, in some cases, opposite (right-left - RL) direction. Moreover, we also considered all the enzymes catalyzing reactions of unknown (UN) direction. Since it is possible that enzyme annotation is available only for parent reactions, i.e., more generic chemical reactions, we also added parent reactions based on Rhea's hierarchical reaction relationships. For each of the Rhea identities acquired, we extracted the corresponding

human enzyme whenever available. We extracted 1492 enzymes linked to GPCR ligands, which were filtered according to the following Gene Ontology cellular components terms: *'plasma membrane', 'axon terminus', 'external side of plasma membrane', 'extracellular', 'neuron projection', 'channel', 'membrane transport'*. We also included in our composite filter additional annotation terms from Pfam[37], Panther classification[38], Gene ontology processes (GO)[39] or full UniProt[40] enzyme name to filter out enzymes classified as kinases, channels, transporters, cytochromes and adenylyl cyclases. We also included rate-limiting enzymes, by mapping 3k human enzymes from RheaDB onto Reactome pathways from 'Metabolism' domain (R-HSA-1430728), which were first filtered, using similar class and domain annotations as above, to exclude kinases, channels, transporters, cytochromes and adenylyl cyclases resulting in a total of 2261 unique enzymes, out of which 945 were found to match 163 pathways involving GPCR ligands. To determine which of these enzymes were rate-limiting the whole biosynthetic pathway, we retrieved for each of them the number of PubMed articles using the following search query: '{Enzyme gene symbol} AND (rate limiting OR bottleneck)'. The enzyme with the highest number of PubMed references for each metabolism pathway associated to GPCR ligands was retained (Table S12).

After these filtering steps, we yielded a total list of 266 enzymes, each involved in interaction with one or multiple GPCRs mediated by synthesized ligands. Receptor-enzymes were further filtered out by using the STRING database, a knowledgebase of known or predicted protein-protein functional interactions[41]. Via STRING, we mapped all possible interactions between GPCRs and enzymes producing cognate ligands, by using a minimum confidence score of 150, and leading to a shortlist of 82 enzymes. The final network contained 82 enzymes, 328 ligands and 243 receptors, for a total of 150 binary enzymes-ligand interactions, 646 ligand-GPCR, and 288 receptor-enzyme (ligand-mediated) interactions.

The whole network has been compiled containing different descriptions of each of the three main interactors and their interactions are currently being deposited to SIGNOR[42] database thanks to an ongoing dedicated curation project.

We generated G protein specific gene set as well as annotations by gathering consensus experimental transducer data (i.e., Universal Coupling Map[9]) as well as predicted through Precogx[7].

Transcriptomics Dataset

We considered gene-level expressions from the dataset 'TCGA TARGET GTEx' publicly available at UCSC Xena (https://xenabrowser.net/datapages/)[43]. These data were generated using the TOIL pipeline, a portable, open-source workflow software that can be used to run scientific workflows on a large scale in cloud or high-performance computing (HPC) environments[44]. The Toil pipeline uses STAR[45] to generate alignments and read coverage graphs, and performs quantification using RSEM[46] and Kallisto[47]. It was utilized to process ~20,000 RNA-seq samples to create a consistent meta-analysis of datasets free of computational batch effects.

We extracted the gene-level expression data, *RSEM expected_count*, using the R package 'UCSCXenatools' for 19109 samples. Thereafter, the TARGET samples were filtered and only TCGA and GTEx samples were retained (n=18305; Table S2). Due to unavailability of GTEx data for all the tissue types, only 16 whole cancer-types (TCGA) were contrasted to the healthy samples pertaining to the same tissue (GTEx). The information for 76 distinct TCGA subtypes was retrieved from TCGAbiolinks[48] (R4.2, Bioconductor v3.16) except for 'Pancreas' and 'Testis' for whom it was unavailable.

For pancreatic cancer we employed a new classification of TCGA samples using a multi-class classifier already implemented to classify three novel PDAC subtypes (Glandular, GL; Transitional, TR; Undifferentiated, UN) obtained from the transcriptional profiles of multiple morphological distinguishable tumor areas isolated by laser micro-dissection (LMD) in primary PDACs of treatment-naïve patients[49]. Briefly, a random Forest (RF) classification method was used to build the model setting the number of trees to 500. To avoid overfitting issues, the k-fold cross validation was performed. A selection procedure to maintain only the most informative features was implemented using the recursive feature elimination (rfe) function in caret R package (https://topepo.github.io/caret/). The gene expression and clinical data of the TCGA study cohort were obtained by the GDC database and then the samples were further selected for PDAC diagnosis. Read counts were normalized using DEseq2's median of ratios. Normalized counts were Log2-transformed and were preprocessed by centering and scaling samples using the Tidymodels R package (https://github.com/tidymodels). PDAC subtypes were predicted in each TCGA sample using the model originated above with the predict function in the randomForest R package setting the parameter type to "class".

Differential Expression Analysis

We obtained log-transformed gene-level count data (RSEM expected_count) from the UCSCXenatools[43], which was subsequently inverse-transformed to raw expected count. TCGA matched normal samples were discarded, and a differential expression (DE) analysis was performed to identify genes with significant expression changes across TCGA-GTEx

samples. The DE analysis was conducted using DESeq2[50], a widely used pipeline for DE analysis. We considered genes with an |LFC|>1 and an adjusted p-value (Padj) < 0.01 (Benjamini-Hochberg correction[51]) to be differentially expressed. This process was performed for each of the 16 whole tissue types and 79 subtypes. The contrast for each whole tissue, or subtype, was performed using the corresponding GTEx whole tissue dataset.

Co-regulation Analysis

To identify co-differentially regulated receptor-ligand pairs, we assigned scores to each of these gene pairs. We considered three major cases: (a) both co-recurrently up/downregulated with significant Padj values (a score of -2/+2), (b) both co-recurrently up/downregulated with at least one of them having a significant Padj value (a score of -1/+1), and (c) no or anti co-differential regulation (a score of 0). This information was displayed in the form of Seaborn clustermap (v0.11.2, Python v3.9.7) with hierarchical clustering performed using the 'ward' method of the scipy.cluster library (v1.7.1, Python v3.9.7). On top of this heatmap, G-coupling information (ref Methods section GPCR - G Protein coupling data) and ligand's mechanism of action (from IUPHAR) was annotated as separate heat maps using matploltib library (v3.4.3, , Python v3.9.7) This way we identified differentially expressed genes and co-differentially regulated receptor-ligand pairs in a comprehensive and robust manner. The use of DESeq2 and Benjamini-Hochberg correction ensured the statistical significance of the results, and the consideration of multiple tissue types and subtypes allowed for a more nuanced understanding of the data.

Gene-Set Enrichment Analysis (GSEA)

We performed gene set enrichment analysis (GSEA) using the WEB-based GEne SeT AnaLysis Toolkit (WebGestalt)[52]. The GSEA process was automated using the R package WebGestaltR. We chose the 'reactome' pathway database[53] for enrichment analysis. The results from these analyses were employed to correlate the DE genes to various reactome pathway gene sets with a positive (enriched in TCGA) or negative enrichment (enriched in GTEx) score with Padj<0.01. We considered GSEA results for downstream analyses by filtering pathways containing the GPCR ligands or enzymes belonging to either Signal transduction ('signaling by GPCR':R-HSA-372790) or Metabolism ('metabolism':R-HSA-1430728) reactome upper level domains.

Comparative Transcriptome-Metabolome analysis

We mapped differentially expressed transcripts and metabolites onto a functional interaction network from Reactome pathways[5455], which integrates in the same network information

from proteins and small organic molecules. We first collected data from the Pan-Cancer Metabolism Data Explorer[22], a comprehensive database that contains information about the differential regulation of metabolites associated with cancer aggressiveness. This resource gathered data from over 900 patient samples from five subtypes of cancer: Breast (BRCA), Prostate (PRAD), Pancreas (PAAD), Kidney (KIRC) and Bladder (BLCA). Using this data, we identified the differential expression regulation of enzyme(s) associated with ligand biosynthesis. For this purpose, we used the list of our curated enzymes to query within this external dataset using an HMDB to ChEBI mapping done via MetaboAnalyst[56]. Then, for each pathway, the LFC and Padj values of constituent enzymes were retrieved. Subsequently, this information was merged with the Reactome functional interaction network for a ligand-receptor signaling pathway to complete the entire axis. This was achieved by considering only the first neighbors for involved participants. The resultant networks were used to visualize the directional regulation as well as the DE profiles by utilizing Cytoscape[57].

Pathway Abundance Score

We compared the enrichment scores of differentially expressed (DE) transcripts with the differential abundance scores of DE metabolites obtained from the Pan-Cancer Metabolism Data Explorer. To this end, we respectively calculated the GSEA Enrichment Score (ES) and the Pathway Abundance Score (PAS)[22] by considering only the filtered set of curated biosynthetic pathways from Reactome, specifically for metabolism (R-HSA-1430728). The PAS was calculated by using the formula (I-D)/S, where I represents the number of metabolites (or enzymes) upregulated (LFC>0) in a pathway, D represents the number of metabolites downregulated (LFC<0) in the pathway, and S is the sum of I and D or 1 if I+D=0. A pathway is considered enriched in cancer if the PAS is positive and negative otherwise (similar to ES). We utilized these two metrics to qualitatively evaluate the concordance of enriched biosynthetic pathways in our findings.

Survival Analysis

The study used univariate unadjusted Cox-Proportional Hazard (Cox-PH) regression models to compute hazard ratios (HR) for predicting the risks of death between high-risk and low-risk TCGA patient groups based on overall survival time. The survival and censoring information was retrieved using TCGAbiolinks for 28 TCGA tissues and 118 subtypes. The risk groups were stratified based on median values of expression, and Kaplan-Meier (KM) plots were used to compare their survival curves. 'survival' (v4.3.0) and 'survminer' packages (v0.4.9) in R (v4.2) were used for survival analyses, and statistical significance between

survival curves was estimated using log-rank tests with p-values less than 0.05 considered significant.

For the individual components (i.e., Receptors/Ligands/Enzymes), patients were stratified in two risk groups based on the median expression value of each component and HR were estimated. Using the 'low expression' group as reference for HR calculations, we label the resulting risk groups as 'High Survival' (HR>1) or 'Low Survival' (0<HR<1). We further employed the combined expression levels for GPCR axes components i.e., GPCR-ligand/GPCR-enzyme for risk stratification. The patients were now stratified in the two risk groups utilizing the median cutoffs of both the components for e.g., for a GPCR-Ligand based stratification, patients with expression value, EV>MedianGPCR and EV>MedianLigand were placed in one group and the patients with EV<MedianGPCR and EV<MedianLigand in another group. We then filtered out those significant GPCR-axis pairs wherein the Hazard-Ratio axis (HR_{axis}) was more than two-fold of the HR in both the individual stratifications (i.e., for above example [$HR_{axis}/HR_{GPCR}<0.5$ or $HR_{axis}/HR_{GPCR}>2$] and [$HR_{axis}/HR_{Ligand}<0.5$ or $HR_{axis}/HR_{Ligand}>2$]) along with the criteria that the logrank-p_{axis} is smaller than the logrank-p values value of both of the individual stratifications and significant i.e., logrank-$p_{axis}<0.05$. These instances were then displayed on a heatmap created using Seaborn scatterplot created using matplotlib (v3.4.3, , Python v3.9.7) with hierarchical clustering performed using the 'ward' method of the scipy.cluster library (v1.7.1, Python v3.9.7).

Survival analyses were performed considering whole cancer tissues, as defined in Xena browser, or at the TCGA molecular subtype level.

Analysis of GPCR drugs on PRISM drug repurposing resource

We retrieved GPCR ligands with cancer growth-inhibitory capacity from a publicly available resource, i.e., PRISM (Program for Response to Inter- and Intra-Species Variation in Cancer Pharmacology)[26]. This drug repurposing resource was developed to identify potential drugs for cancer treatment. To predict drug response, PRISM utilizes genomic data from cancer cell lines and patient-derived xenografts, which are inputted into machine learning pipelines. By taking into account inter- and intra-species variability in drug response, PRISM aims to provide personalized treatment options for specific cancer subtypes. The dataset retrieved from PRISM contained information on the growth-inhibitory activity of over 4,500 drugs tested on 578 human cancer cell lines. This data was filtered based on the drugs which had GPCRs as targets and a list of 52 GPCR drugs/ligands was obtained. To identify active drugs for cancer treatment, PRISM uses the bimodality coefficient and correlation as metrics. The bimodality coefficient measures the separation between the two peaks in a drug response distribution, identifying drugs with a bimodal distribution of response across cancer

cell lines. The correlation measures the strength of the relationship between predicted and actual drug response in patient-derived xenograft models. Following a similar approach, we used these metrics (correlation>0.2, bimodality coefficient>0.35) to identify GPCR drugs that are active against specific cancer subtypes. The active drugs were then investigated on the basis of GPCRs associated with survival in either of GPCR-Ligand or GPCR-Enzyme axes. The information was further annotated with G-coupling information and ultimately displayed using visual representations such as scatter plots, venn diagram and heatmaps utilizing seaborn (v0.11.2, Python v3.9.7) and matplotlib libraries (v3.4.3, , Python v3.9.7).

Availability

Code and data used for this study are available at: https://gpcrcanceraxes.bioinfolab.sns.it/

Conflict of interest

JSG reports consulting fees from Domain Pharmaceuticals, Pangea Therapeutics, and io9, and is founder of Kadima Pharmaceuticals, all unrelated to the current study.

Funding

F.R. was supported by the Italian Ministry of University and Research through the Department of excellence “Faculty of Sciences” of Scuola Normale Superiore. The research leading to these results also received funding from the Italian Association for Cancer Research (AIRC) under My First AIRC Grant (MFAG) 2020 - ID. 24317 project – P.I. F.R; the US National Institutes of Health (U24 HG012198) to G.W.

Acknowledgments

We gratefully acknowledge the CINECA award, in collaboration with AIRC, for the availability of high performance computing resources and support. We gratefully acknowledge computational resources of the Center for High Performance Computing (CHPC) at Scuola Normale Superiore.

Figures

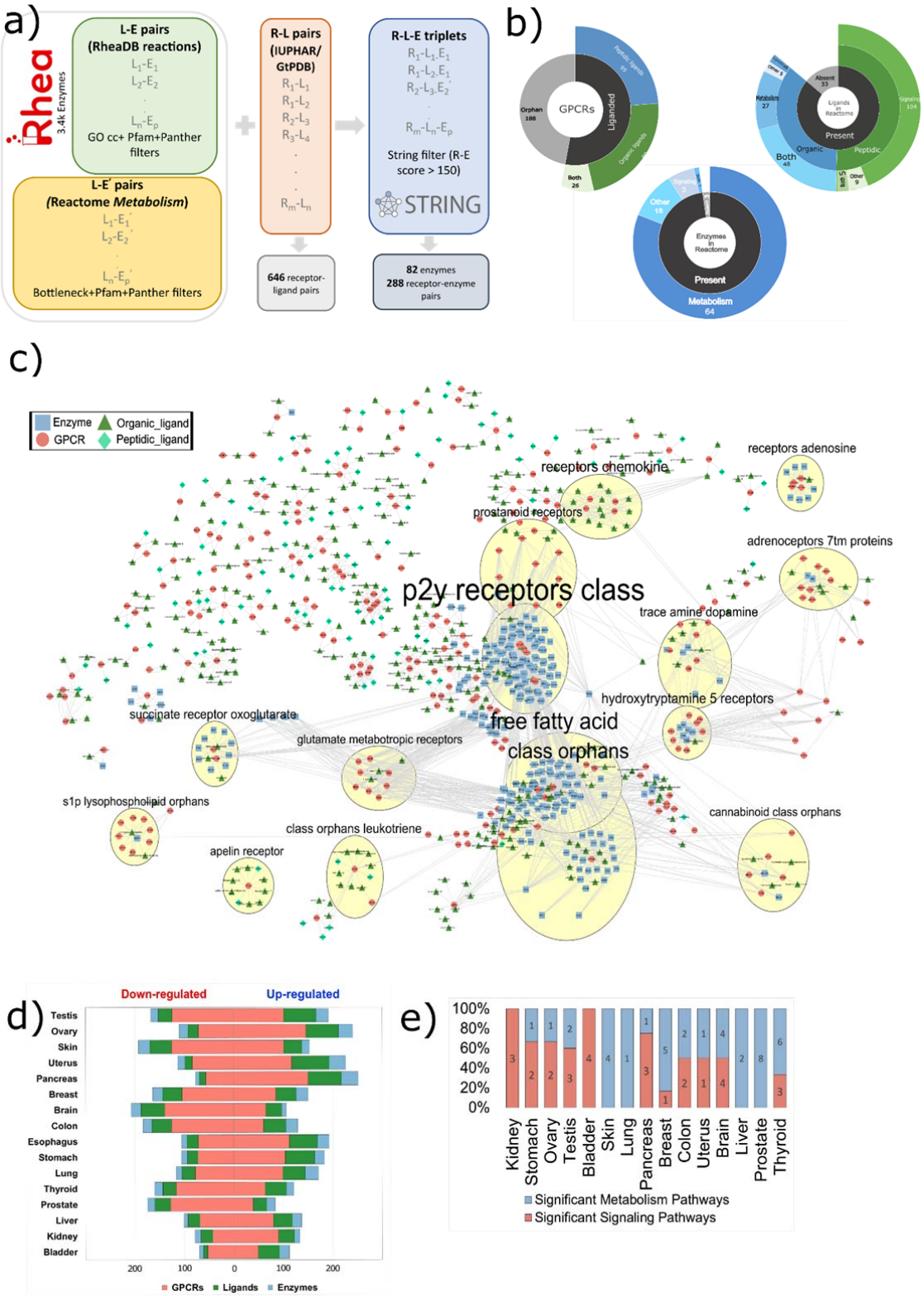

Figure 1

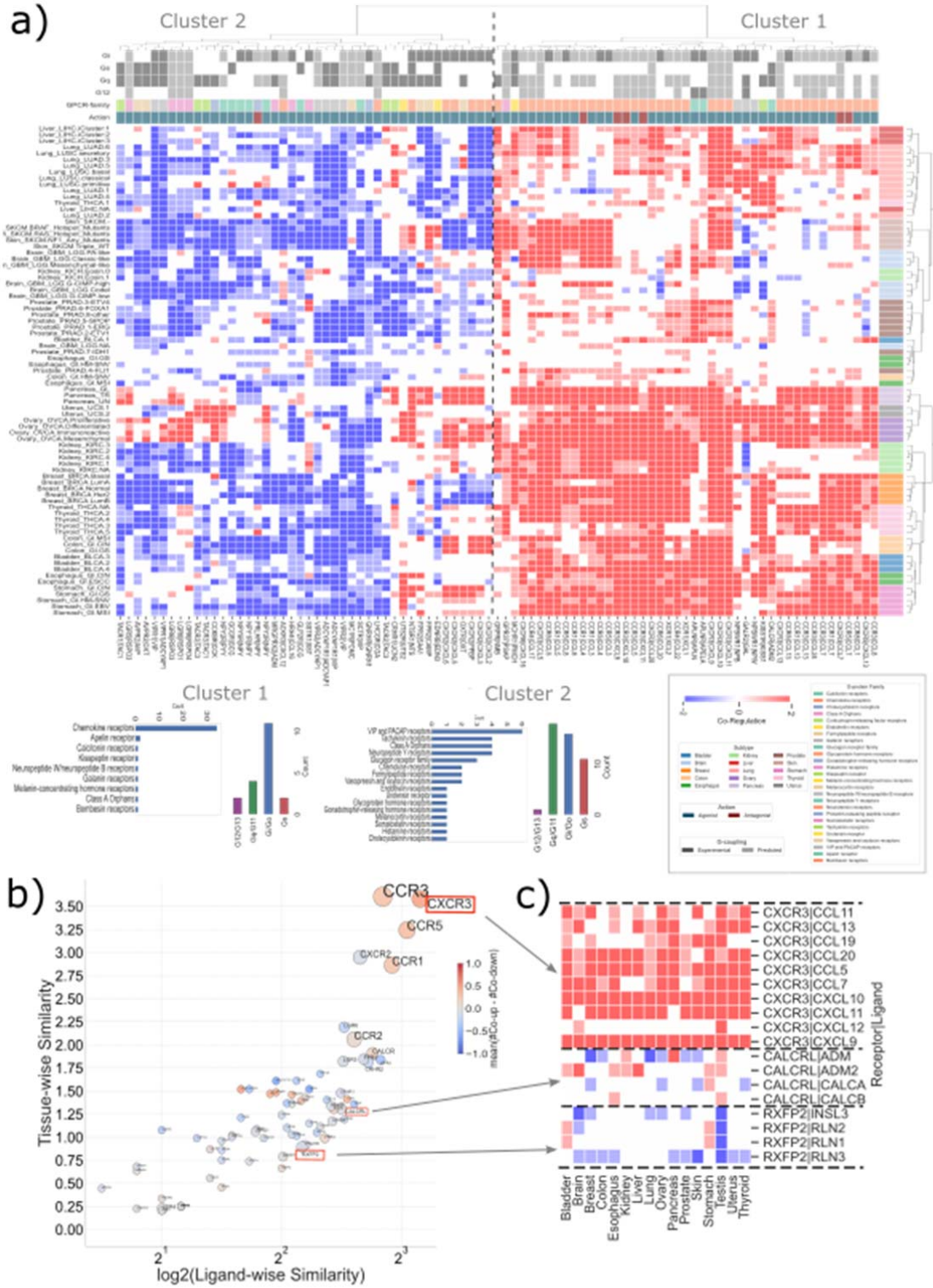
a)
Cluster 2
Cluster 1
Cluster 1
Cluster 2
b)
CCR3
CXCR3
CCR5
CXCR2
CCR1
CCR2
Tissue-wise Similarity
log2(Ligand-wise Similarity)
c)
CXCR3|CCL11
CXCR3|CCL13
CXCR3|CCL19
CXCR3|CCL20
CXCR3|CCL5
CXCR3|CCL7
CXCR3|CXCL10
CXCR3|CXCL11
CXCR3|CXCL12
CXCR3|CXCL9
CALCRL|ADM
CALCRL|ADM2
CALCRL|CALCA
CALCRL|CALCB
RXFP2|INSL3
RXFP2|RLN2
RXFP2|RLN1
RXFP2|RLN3
Receptor|Ligand
Bladder
Brain
Breast
Colon
Esophagus
Kidney
Liver
Lung
Ovary
Pancreas
Prostate
Skin
Stomach
Testis
Uterus
Thyroid

Figure 2

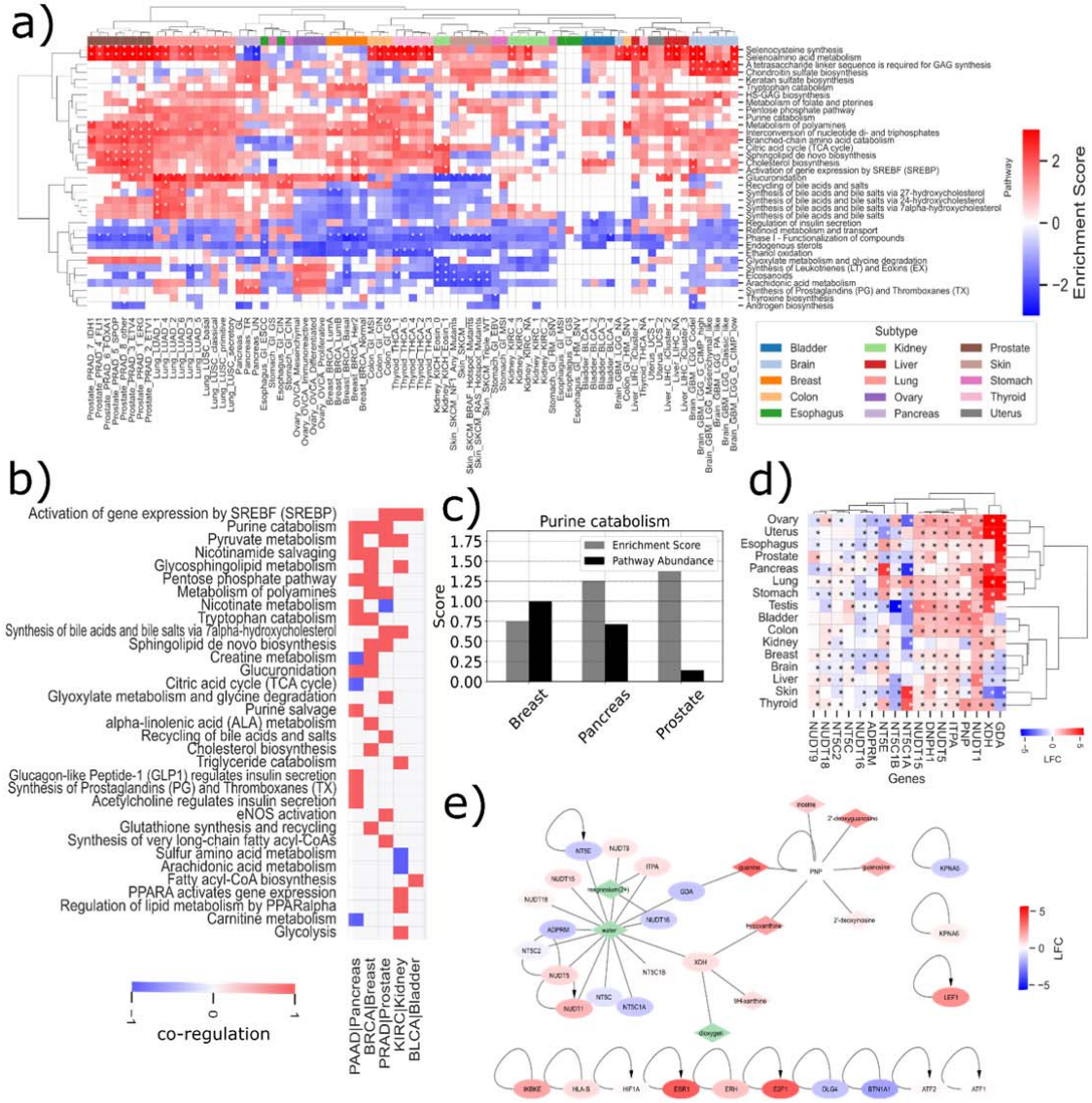
a)
Selenocysteine synthesis
Selenoamino acid metabolism
A tetrasaccharide linker sequence is required for GAG synthesis
Chondroitin sulfate biosynthesis
Keratan sulfate biosynthesis
Tryptophan catabolism
HS-GAG biosynthesis
Metabolism of folate and pterines
Pentose phosphate pathway
Purine catabolism
Metabolism of polyamines
Interconversion of nucleotide di- and triphosphates
Branched-chain amino acid catabolism
Citric acid cycle (TCA cycle)
Sphingolipid de novo biosynthesis
Cholesterol biosynthesis
Activation of gene expression by SREBF (SREBP)
Glucuronidation
Recycling of bile acids and salts
Synthesis of bile acids and bile salts via 27-hydroxycholesterol
Synthesis of bile acids and bile salts via 24-hydroxycholesterol
Synthesis of bile acids and bile salts via 7alpha-hydroxycholesterol
Synthesis of bile acids and bile salts
Regulation of insulin secretion
Retinoid metabolism and transport
Phase I - Functionalization of compounds
Endogenous sterols
Ethanol oxidation
Glyoxylate metabolism and glycine degradation
Synthesis of Leukotrienes (LT) and Eoxins (EX)
Eicosanoids
Arachidonic acid metabolism
Synthesis of Prostaglandins (PG) and Thromboxanes (TX)
Thyroxine biosynthesis
Androgen biosynthesis
Pathway
Enrichment Score
Subtype
Bladder
Brain
Breast
Colon
Esophagus
Kidney
Liver
Lung
Ovary
Pancreas
Prostate
Skin
Stomach
Thyroid
Uterus
b)
Activation of gene expression by SREBF (SREBP)
Purine catabolism
Pyruvate metabolism
Nicotinamide salvaging
Glycosphingolipid metabolism
Pentose phosphate pathway
Metabolism of polyamines
Nicotinate metabolism
Tryptophan catabolism
Synthesis of bile acids and bile salts via 7alpha-hydroxycholesterol
Sphingolipid de novo biosynthesis
Creatine metabolism
Glucuronidation
Citric acid cycle (TCA cycle)
Glyoxylate metabolism and glycine degradation
Purine salvage
alpha-linolenic acid (ALA) metabolism
Recycling of bile acids and salts
Cholesterol biosynthesis
Triglyceride catabolism
Glucagon-like Peptide-1 (GLP1) regulates insulin secretion
Synthesis of Prostaglandins (PG) and Thromboxanes (TX)
Acetylcholine regulates insulin secretion
eNOS activation
Glutathione synthesis and recycling
Synthesis of very long-chain fatty acyl-CoAs
Sulfur amino acid metabolism
Arachidonic acid metabolism
Fatty acyl-CoA biosynthesis
PPARA activates gene expression
Regulation of lipid metabolism by PPARalpha
Carnitine metabolism
Glycolysis
co-regulation
PAAD|Pancreas
BRCA|Breast
PRAD|Prostate
KIRC|Kidney
BLCA|Bladder
c)
Purine catabolism
Enrichment Score
Pathway Abundance
Score
Breast
Pancreas
Prostate
d)
Ovary
Uterus
Esophagus
Prostate
Pancreas
Lung
Stomach
Testis
Bladder
Colon
Kidney
Breast
Brain
Liver
Skin
Thyroid
Genes
LFC
e)
LFC

Figure 3

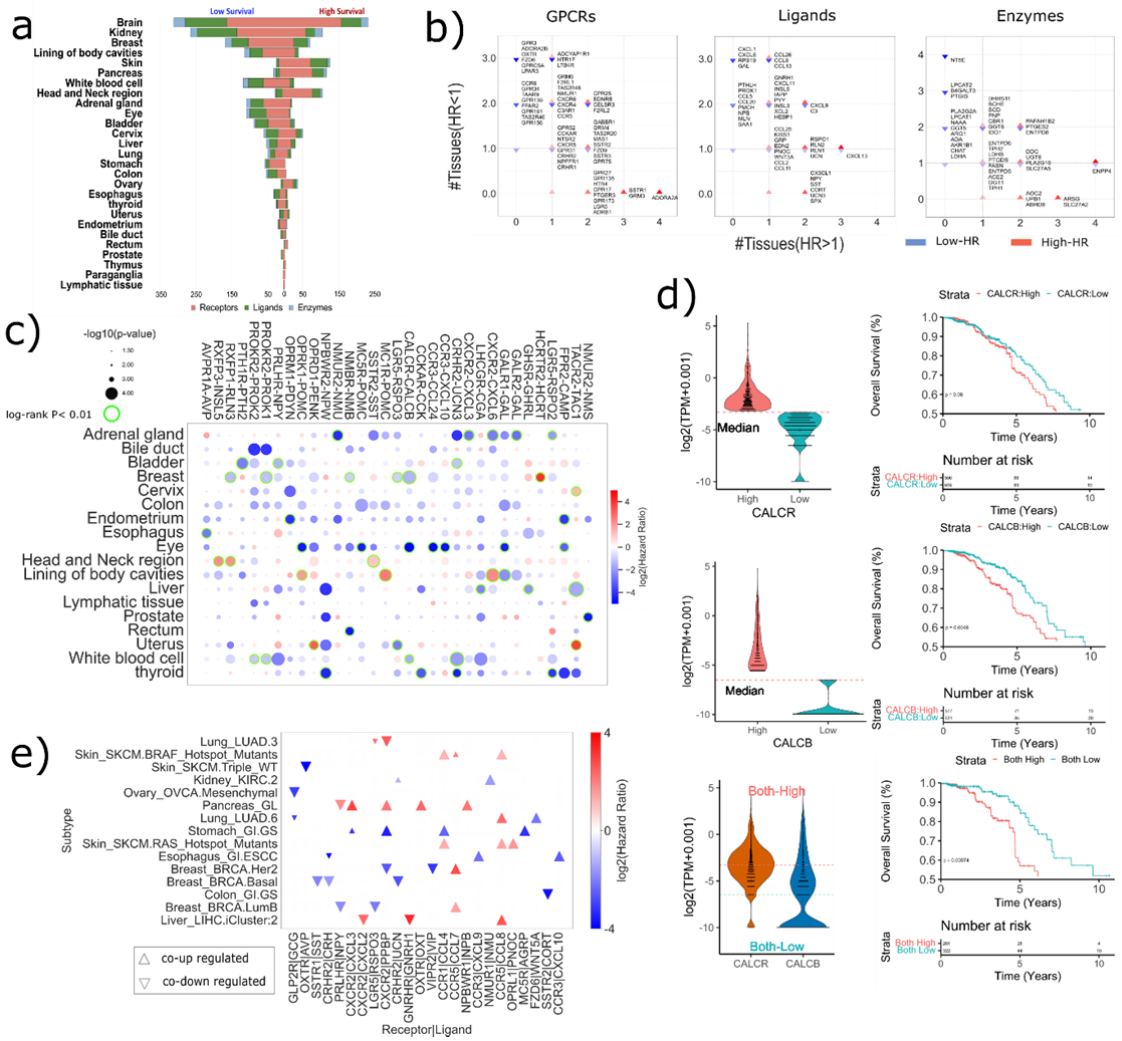
a
Low Survival
High Survival
Brain
Kidney
Breast
Lining of body cavities
Skin
Pancreas
White blood cell
Head and Neck region
Adrenal gland
Eye
Bladder
Cervix
Liver
Lung
Stomach
Colon
Ovary
Esophagus
thyroid
Uterus
Endometrium
Bile duct
Rectum
Prostate
Thymus
Paraganglia
Lymphatic tissue
Receptors
Ligands
Enzymes
b)
GPCRs
Ligands
Enzymes
#Tissues(HR<1)
#Tissues(HR>1)
Low-HR
High-HR
c)
-log10(p-value)
log-rank P< 0.01
log2(Hazard Ratio)
d)
Strata
CALCR:High
CALCR:Low
CALCB:High
CALCB:Low
Both High
Both Low
Median
Both-High
Both-Low
log2(TPM+0.001)
Overall Survival (%)
Time (Years)
Number at risk
CALCR
CALCB
e)
Subtype
Lung_LUAD.3
Skin_SKCM.BRAF_Hotspot_Mutants
Skin_SKCM.Triple_WT
Kidney_KIRC.2
Ovary_OVCA.Mesenchymal
Pancreas_GL
Lung_LUAD.6
Stomach_GI.GS
Skin_SKCM.RAS_Hotspot_Mutants
Esophagus_GI.ESCC
Breast_BRCA.Her2
Breast_BRCA.Basal
Colon_GI.GS
Breast_BRCA.LumB
Liver_LIHC.iCluster:2
co-up regulated
co-down regulated
log2(Hazard Ratio)
Receptor|Ligand

Figure 4

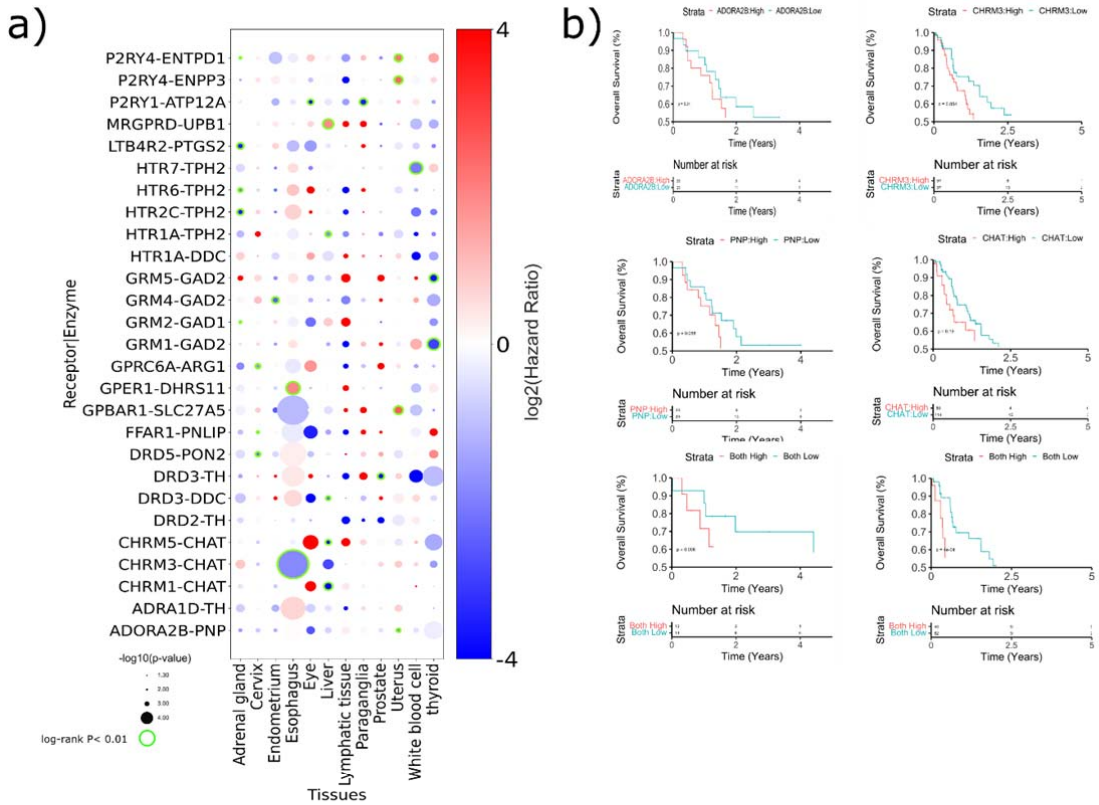
a)
b)
P2RY4-ENTPD1
P2RY4-ENPP3
P2RY1-ATP12A
MRGPRD-UPB1
LTB4R2-PTGS2
HTR7-TPH2
HTR6-TPH2
HTR2C-TPH2
HTR1A-TPH2
HTR1A-DDC
GRM5-GAD2
GRM4-GAD2
GRM2-GAD1
GRM1-GAD2
GPRC6A-ARG1
GPER1-DHRS11
GPBAR1-SLC27A5
FFAR1-PNLIP
DRD5-PON2
DRD3-TH
DRD3-DDC
DRD2-TH
CHRM5-CHAT
CHRM3-CHAT
CHRM1-CHAT
ADRA1D-TH
ADORA2B-PNP
Receptor|Enzyme
Adrenal gland
Cervix
Endometrium
Esophagus
Eye
Liver
Lymphatic tissue
Paraganglia
Prostate
Uterus
White blood cell
thyroid
Tissues
log2(Hazard Ratio)
4
0
-4
-log10(p-value)
log-rank P< 0.01
Strata - ADORA2B:High - ADORA2B:Low
Strata - CHRM3:High - CHRM3:Low
Strata - PNP:High - PNP:Low
Strata - CHAT:High - CHAT:Low
Strata - Both High - Both Low
Overall Survival (%)
Time (Years)
Number at risk

Figure 5

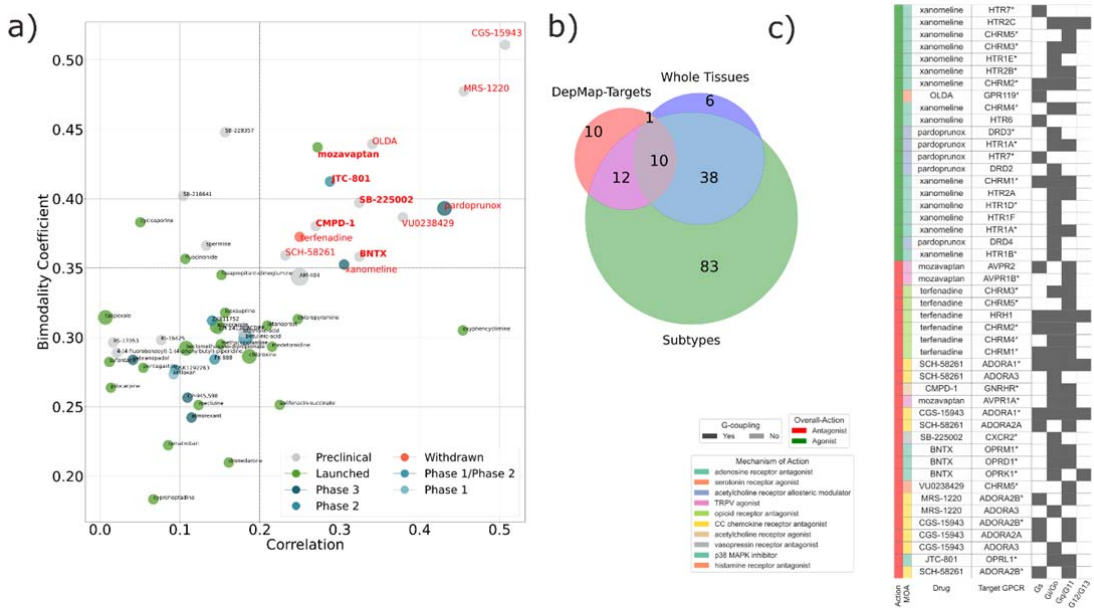
a)
b)
c)
Bimodality Coefficient
Correlation
CGS-15943
MRS-1220
OLDA
mozavaptan
JTC-801
SB-225002
pardoprunox
CMPD-1
VU0238429
terfenadine
SCH-58261
BNTX
xanomeline
Preclinical
Launched
Phase 3
Phase 2
Withdrawn
Phase 1/Phase 2
Phase 1
DepMap-Targets
Whole Tissues
Subtypes
G-coupling
Yes
No
Overall-Action
Antagonist
Agonist
Mechanism of Action
adenosine receptor antagonist
serotonin receptor agonist
acetylcholine receptor allosteric modulator
TRPV agonist
opioid receptor antagonist
CC chemokine receptor antagonist
acetylcholine receptor agonist
vasopressin receptor antagonist
p38 MAPK inhibitor
histamine receptor antagonist
Action MOA
Drug
Target GPCR
Gs
Gi/Go
Gq/G11
G12/G13

Figure 6

Figure Legends

Figure 1 GPCR extracellular signaling network and overview of the datasets considered a) workflow of the procedure to generate enzyme-receptor interacting pairs; b) Sunburst charts providing an overview of the number of liganded and orphan G-protein-coupled receptors (GPCRs) considered; Classification of the liganded GPCRs based on their ligand type, i.e., either peptide, organic, or a combination of both; number of enzymes that are either currently included or absent within the Reactome pathways. The included ligands are additionally subcategorized based on the frequency of their types and the frequency of the Reactome pathway domains with which they are linked. For enzymes, only the second layer of this information is shown; c) The network of GPCRs and cognate ligands and biosynthetic enzymes; d) Bar plot exhibiting the frequency of differentially expressed (TCGA vs. GTEx) GPCRs, ligands, and enzymes corresponding to each whole tissue. e) Stacked bar-plot displaying the number of significantly enriched ligand-associated pathways within Reactome sub-domains: Signaling ('R-HSA-372790: signaling by GPCR') and Metabolism ('R-HSA-1430728:metabolism').

Figure 2 Peptide Ligand-Receptor co-regulation a) Heatmap (center panel) displaying the co-differential regulation for Receptor-Ligand pairs across different TCGA subtypes (color-coded at the top row). Darker red represents both receptor and ligand significantly co-up regulated in TCGA (i.e., LFC>1 and Padj<0.01) and darker blue represents both receptor and ligand significantly co-down regulated in TCGA (i.e., LFC<1 and Padj<0.01). Paler colors represent either of the receptor-ligand as significantly DE (i.e., |LFC|>1 for both but Padj<0.01 for only one of these). White cells indicate anti-regulation or no fold change at all in at least one of them. Only pairs affected in at least 25% of TCGA subtypes are displayed. A dashed line separating the two clusters, created using Hierarchical clustering, is shown in the middle. Heatmap (left panel) uses color codes to display the ligand's mechanism of action in 'Action', G Protein-coupling associated with the GPCRs and GPCR Family. Heatmap (right panel) displays the information contained in the left panel as concise bar plots for each of the two clusters. For each cluster barplots indicate G-protein coupling preferences as well as GPCR families; b) The scatter plot displays a GPCR-centric view of the heatmap in (a) based on tissue-wise or ligand-wise similarity. Here, ligand-wise similarity for each GPCR is the average of the pairwise Euclidean distances between co-differentially expressed (co-DE) profiles across its ligands (i.e., vertically), while tissue-wise similarity is a similar metric across tissues (i.e., horizontally). The size of the markers is proportional to the number of ligands, and the colors correspond to the average difference in the number of co-up and co-down profiles. GPCRs located in the top-right corner are more diverse in terms of their ligand interactions; c) Diverse co-DE profiles are observed with respect to different ligands and tissues corresponding to the same GPCR. For example, CXCR3 and its corresponding ligands exhibit an almost exclusively co-upregulated profile irrespective of tissue type, while CALCRL and its ligands display varied co-regulation profiles, implying a varying interaction with its ligands in different tissue (or cancer) types.

Figure 3: **Biosynthetic pathway enrichment** (a) Heatmap of GSEA pathway enrichment analysis for differentially expressed (DE) genes in cancer (TCGA) over normal (GTEx) samples, considering Reactome pathways related to signaling and metabolism. Red cells indicate pathways enriched in TCGA, blue cells indicate pathways enriched in GTEx, and

white cells indicate no enrichment. Cells marked with '*' correspond to a statistically significant enrichment (Padj < 0.01).
(b) Concordant pathway enrichment analysis considering both DE genes (Enrichment Score, ES) and metabolites (Pathway Abundance Score, PAS). A score of 1 (red) indicates co enrichment in cancer (ES & PAS > 0), and a score of -1 (blue) indicates co enrichment in normal samples (ES & PAS < 0).
(c) Bar plot displaying numerical values for ES and PAS for the 'Purine catabolism' pathway in three different tissues: Breast, Bladder, and Prostate.
(d) Heatmap of DE genes for the 'Purine catabolism' pathway in Breast cancer. Red cells indicate upregulated genes in TCGA, blue cells indicate downregulated genes in TCGA, and cells marked with '*' correspond to a statistically significant differential expression (Padj < 0.01).
(e) A functional interaction network between genes (ovals) and metabolites (diamonds) in the 'Purine catabolism' pathway in Breast cancer. Red nodes indicate upregulated components, blue nodes indicate downregulated components, and green nodes indicate no information available. The network shows that over-activation of the pathway is contributed by over-expression of both genes and metabolites.

Figure 4 Association of GPCR-peptide axes to survival (a) Survival association of G protein-coupled receptor (GPCR) components in various cancer types. The funnel plot shows the number of significant instances of individual components, such as receptors, ligands, and enzymes, whose expression values are associated with patient survival across various cancer types. A total of 302 unique significant receptor instances (log rank p-value < 0.05, FDR<0.1) were identified in 11 cancer tissues, 103 ligands in 10 cancers, and 71 enzymes in 10 cancers. (b) Scatterplots for individual receptor instances, enzymes and ligands associated with patient survival in various cancer types. (logrank-p<0.05, FDR<0.1). x-axis displays the number of tissues in which the genes are associated with lower survival (inverted blue triangles) and, vice-versa, y-axis displays the number of tissues in which the genes are associated with higher survival (red triangles). Only the genes which are significantly associated with survival in at-least two tissues are shown. c) The bubble plot shows the correlation between the combined-expression levels of GPCR-ligand pairs and patient survival across various cancer types. The pairs with a log rank p-value <0.05 and also lower than log rank p-values for individual GPCR/ligand are displayed. Bubble color is proportional to HR: i.e., HR>1 : High expression is correlated with high survival (red); HR<1: High expression is correlated with poor survival (blue). Bubble diameters are proportional to the -log10(log-rank p-value). Green highlighted bubbles represent the most significant instances (sample sizes>5, FDR<0.1). (d) The expression values for the CALCR-CALCB axes in breast cancer (right) and corresponding Kaplan-Meier curve for survival analysis of patients stratified based on the individual as well as combined receptor/ligand expression;(e) Scatter-plot showing with differentially co-expressed GPCR-ligand pairs (upper triangle=co-up regulation; lower triangle=co-down regulation) that were significantly associated with patient survival (red=higher survival; blue=lower survival). A total of 24 receptor-ligand pairs from 15 cancer subtypes were identified.

Figure 5 (a) The bubble plot shows the correlation between the combined-expression levels of GPCR-enzyme pairs and patient survival across various cancer types. The pairs with a log rank p-value <0.05 and also lower than log rank p-values for individual GPCR/enzyme are displayed. Further, the pairs with rate-limiting enzymes having less than 100 PubMed

references are not shown. Bubble color is proportional to HR: i.e., HR>1 : High expression is correlated with high survival (red); HR<1: High expression is correlated with poor survival (blue). Bubble diameters are proportional to the -log(log-rank p-value). Green highlighted bubbles represent the most significant instances (sample sizes>5, FDR<0.1). (b) The CHRM3-CHAT axis is recurrently correlated with lower survival rates in Esophageal cancer. The KM plots (left) display the risk enhancement achieved when CHRM3-CHAT combined stratification was applied as compared to individual CHRM3/CHAT as evident by log rank p-values. Similarly, the ADORA2B-PNP axis is also consistently associated with lower survival rates in Uterine cancer, as evident from the KM plot on the right.

Figure 6 GPCR ligands with cancer growth-inhibitory capacity (a) The scatterplot displays 52 GPCR ligands that were tested in 578 cell lines in PRISM drug repurposing resource.13 GPCR ligands (in red) were found to significantly inhibit the growth of cancer cell lines (correlation>0.2, bimodality coefficient>0.35). (b) Venn diagram showing the overlap of GPCRs in the target proteins of these 13 ligands with the pooled list of GPCRs that were found to mediate survival associated GPCR-ligand/GPCR-enzyme axes. (c) The heatmap displays the 13 shortlisted ligands and their corresponding GPCR targets. The targets marked with '*' are the overlapping GPCRs with significant axes. Heatmap also displays the overall action mode of ligand, more detailed mechanism of action (MOA) and G-protein coupling associated with the GPCR.

References

1. Pierce, K. L., Premont, R. T. & Lefkowitz, R. J. Seven-transmembrane receptors. *Nat Rev Mol Cell Biol* **3**, 639–50 (2002).
2. Oldham, W. M. & Hamm, H. E. Heterotrimeric G protein activation by G-protein-coupled receptors. *Nat Rev Mol Cell Biol* **9**, 60–71 (2008).
3. Wootten, D., Christopoulos, A., Marti-Solano, M., Babu, M. M. & Sexton, P. M. Mechanisms of signalling and biased agonism in G protein-coupled receptors. *Nat Rev Mol Cell Biol* 1 (2018) doi:10.1038/s41580-018-0049-3.
4. de Mendoza, A., Sebé-Pedrós, A. & Ruiz-Trillo, I. The evolution of the GPCR signaling system in eukaryotes: modularity, conservation, and the transition to metazoan multicellularity. *Genome Biol Evol* **6**, 606–619 (2014).
5. Flock, T. *et al.* Selectivity determinants of GPCR-G-protein binding. *Nature* **545**, 317–322 (2017).
6. Inoue, A. *et al.* Illuminating G-Protein-Coupling Selectivity of GPCRs. *Cell* **177**, 1933-1947.e25 (2019).
7. Matic, M. *et al.* PRECOGx: exploring GPCR signaling mechanisms with deep protein representations. *Nucleic Acids Res* **50**, W598–W610 (2022).

8. Singh, G., Inoue, A., Gutkind, J. S., Russell, R. B. & Raimondi, F. PRECOG: PREdicting COupling probabilities of G-protein coupled receptors. *Nucleic Acids Res* **47**, W395–W401 (2019).
9. Hauser, A. S. *et al.* Common coupling map advances GPCR-G protein selectivity. *Elife* **11**, (2022).
10. Avet, C. *et al.* Effector membrane translocation biosensors reveal G protein and βarrestin coupling profiles of 100 therapeutically relevant GPCRs. *Elife* **11**, 1–34 (2022).
11. Foster, S. R. *et al.* Discovery of Human Signaling Systems: Pairing Peptides to G Protein-Coupled Receptors. *Cell* **179**, 895-908.e21 (2019).
12. O'Hayre, M. *et al.* The emerging mutational landscape of G proteins and G-protein-coupled receptors in cancer. *Nat Rev Cancer* (2013) doi:10.1038/nrc3521.
13. Ramms, D. J. *et al.* Gαs–Protein Kinase A (PKA) Pathway Signalopathies: The Emerging Genetic Landscape and Therapeutic Potential of Human Diseases Driven by Aberrant Gαs-PKA Signaling. *Pharmacol Rev* **73**, 155–197 (2021).
14. Wu, V. *et al.* Illuminating the Onco-GPCRome: Novel G protein-coupled receptor-driven oncocrine networks and targets for cancer immunotherapy. *J Biol Chem* (2019) doi:10.1074/jbc.REV119.005601.
15. Arang, N. & Gutkind, J. S. G Protein-Coupled receptors and heterotrimeric G proteins as cancer drivers. *FEBS Lett* **594**, 4201–4232 (2020).
16. Raimondi, F. *et al.* Rare, functional, somatic variants in gene families linked to cancer genes: GPCR signaling as a paradigm. *Oncogene* **38**, 6491–6506 (2019).
17. Hanahan, D. & Monje, M. Cancer hallmarks intersect with neuroscience in the tumor microenvironment. *Cancer Cell* **41**, 573–580 (2023).
18. Renz, B. W. *et al.* β2 Adrenergic-Neurotrophin Feedforward Loop Promotes Pancreatic Cancer. *Cancer Cell* **33**, 75-90.e7 (2018).
19. Hayakawa, Y. *et al.* Tumorigenesis through Aberrant Cholinergic Article Nerve Growth Factor Promotes Gastric Tumorigenesis through Aberrant Cholinergic Signaling. *Cancer Cell* **31**, 21–34 (2017).
20. Armingol, E., Officer, A., Harismendy, O. & Lewis, N. E. Deciphering cell-cell interactions and communication from gene expression. *Nat Rev Genet* **22**, 71–88 (2021).
21. Dimitrov, D. *et al.* Comparison of methods and resources for cell-cell communication inference from single-cell RNA-Seq data. *Nat Commun* **13**, (2022).
22. Reznik, E. *et al.* A Landscape of Metabolic Variation across Tumor Types. *Cell Syst* **6**, 301-313.e3 (2018).
23. Patra, K. C. *et al.* Mutant GNAS drives pancreatic tumourigenesis by inducing PKA-mediated SIK suppression and reprogramming lipid metabolism. *Nat Cell Biol* **20**, 811–822 (2018).
24. Ideno, N. *et al.* GNASR201C Induces Pancreatic Cystic Neoplasms in Mice That Express Activated KRAS by Inhibiting YAP1 Signaling. *Gastroenterology* (2018) doi:10.1053/J.GASTRO.2018.08.006.
25. Cekic, C. & Linden, J. Adenosine A2A receptors intrinsically regulate CD8+ T cells in the tumor microenvironment. *Cancer Res* **74**, 7239–7249 (2014).
26. Corsello, S. M. *et al.* Discovering the anti-cancer potential of non-oncology drugs by systematic viability profiling. *Nat Cancer* **1**, 235–248 (2020).
27. Ozga, A. J., Chow, M. T. & Luster, A. D. Chemokines and the immune response to cancer. *Immunity* **54**, 859–874 (2021).

28. Larrue, C. *et al.* Adrenomedullin-CALCRL axis controls relapse-initiating drug tolerant acute myeloid leukemia cells. *Nat Commun* **12**, 1–15 (2021).
29. Lechner, M. *et al.* Somatostatin receptor 2 expression in nasopharyngeal cancer is induced by Epstein Barr virus infection: impact on prognosis, imaging and therapy. *Nat Commun* **12**, (2021).
30. Zhao, Y. *et al.* Acetylcholinesterase, a key prognostic predictor for hepatocellular carcinoma, suppresses cell growth and induces chemosensitization. *Hepatology* **53**, 493–503 (2011).
31. Wu VH, Y. B. F. F. S.-K. R. W. Z. W. A. S. M. P. M. C. L. C. J. S. J. M. M. R. F. H. T. B. R. V. D. I.-B. R. C. H. R. E. M. J. G. JS. The GPCR-Gαs-PKA signaling axis promotes T cell dysfunction and cancer immunotherapy failure. *Nat Immunol* **in press**, (2023).
32. Leone, R. D. & Emens, L. A. Targeting adenosine for cancer immunotherapy. *J Immunother Cancer* **6**, 1–9 (2018).
33. Perrot, I. *et al.* Blocking Antibodies Targeting the CD39/CD73 Immunosuppressive Pathway Unleash Immune Responses in Combination Cancer Therapies. *Cell Rep* **27**, 2411-2425.e9 (2019).
34. Harding, S. D. *et al.* The IUPHAR/BPS Guide to PHARMACOLOGY in 2018: updates and expansion to encompass the new guide to IMMUNOPHARMACOLOGY. *Nucleic Acids Res* **46**, D1091–D1106 (2018).
35. Lombardot, T. *et al.* Updates in Rhea: SPARQLing biochemical reaction data. *Nucleic Acids Res* **47**, D596–D600 (2019).
36. Hastings, J. *et al.* ChEBI in 2016: Improved services and an expanding collection of metabolites. *Nucleic Acids Res* **44**, D1214–D1219 (2016).
37. Mistry, J. *et al.* Pfam: The protein families database in 2021. *Nucleic Acids Res* **49**, D412–D419 (2021).
38. Mi, H. *et al.* PANTHER version 16: a revised family classification, tree-based classification tool, enhancer regions and extensive API. *Nucleic Acids Res* **49**, D394–D403 (2021).
39. Blake, J. A. *et al.* Gene ontology consortium: Going forward. *Nucleic Acids Res* **43**, D1049–D1056 (2015).
40. UniProt: the universal protein knowledgebase. *Nucleic Acids Res* **45**, D158–D169 (2017).
41. Szklarczyk, D. *et al.* STRING v11: protein-protein association networks with increased coverage, supporting functional discovery in genome-wide experimental datasets. *Nucleic Acids Res* **47**, D607–D613 (2019).
42. Lo Surdo, P. *et al.* SIGNOR 3.0, the SIGnaling network open resource 3.0: 2022 update. *Nucleic Acids Res* **51**, D631–D637 (2023).
43. Goldman, M. J. *et al.* Visualizing and interpreting cancer genomics data via the Xena platform. *Nat Biotechnol* **38**, 675–678 (2020).
44. Vivian, J. *et al.* Toil enables reproducible, open source, big biomedical data analyses. *Nat Biotechnol* **35**, 314–316 (2017).
45. Dobin, A. *et al.* STAR: ultrafast universal RNA-seq aligner. *Bioinformatics* **29**, 15–21 (2013).
46. Li, B. & Dewey, C. N. RSEM: accurate transcript quantification from RNA-Seq data with or without a reference genome. *BMC Bioinformatics* **12**, (2011).
47. Bray, N. L., Pimentel, H., Melsted, P. & Pachter, L. Near-optimal probabilistic RNA-seq quantification. *Nat Biotechnol* **34**, 525–527 (2016).

48. Colaprico, A. *et al.* TCGAbiolinks: An R/Bioconductor package for integrative analysis of TCGA data. *Nucleic Acids Res* **44**, e71 (2016).
49. Di Chiaro, P. *et al.* Coexisting morpho-biotypes unveil the regulatory bases of phenotypic plasticity in pancreatic ductal adenocarcinoma. doi:10.1101/2022.12.12.520054.
50. Love, M. I., Huber, W. & Anders, S. Moderated estimation of fold change and dispersion for RNA-seq data with DESeq2. *Genome Biol* **15**, 550 (2014).
51. Benjamini, Y. & Hochberg, Y. Controlling the False Discovery Rate: A Practical and Powerful Approach to Multiple Testing. *Journal of the Royal Statistical Society. Series B (Methodological)* vol. 57 289–300 Preprint at https://doi.org/10.2307/2346101 (1995).
52. Wang, J., Duncan, D., Shi, Z. & Zhang, B. WEB-based GEne SeT AnaLysis Toolkit (WebGestalt): update 2013. *Nucleic Acids Res* **41**, (2013).
53. Jassal, B. *et al.* The reactome pathway knowledgebase. *Nucleic Acids Res* **48**, D498–D503 (2020).
54. Wu, G., Feng, X. & Stein, L. A human functional protein interaction network and its application to cancer data analysis. *Genome Biol* **11**, R53 (2010).
55. Raimondi, F., Burkhart, J. G., Betts, M. J., Russell, R. B. & Wu, G. Leveraging biochemical reactions to unravel functional impacts of cancer somatic variants affecting protein interaction interfaces. *F1000Research 2021 10:1111* **10**, 1111 (2021).
56. Xia, J., Psychogios, N., Young, N. & Wishart, D. S. MetaboAnalyst: a web server for metabolomic data analysis and interpretation. *Nucleic Acids Res* **37**, (2009).
57. Lotia, S., Montojo, J., Dong, Y., Bader, G. D. & Pico, A. R. Cytoscape app store. *Bioinformatics* **29**, 1350–1351 (2013).

Supplementary Figures

Figure S1: a) stacked barplot with the distribution of DE GPCRs for each cancer tissue categorized by coupling information; b) heatmap showing the LFCs from DE analysis (TCGA vs GTEX, via DESEQ2) of G protein in each cancer tissue. Significant instances are annotated with "*"; c) same as b) but for cancer molecular subtypes; d) heatmap showing ligand-associated pathways which are significantly enriched in at least one cancer subtype
Figure S2: Heatmap displaying the co-differential regulation for Receptor-Ligand pairs across different TCGA subtypes (color-coded at the top row). Darker red represents both receptor and ligand significantly co-up regulated in TCGA (i.e., LFC>1 and Padj<0.01) and darker blue represents both receptor and ligand significantly co-down regulated in TCGA (i.e., LFC<1 and Padj<0.01). Paler colors represent either of the receptor-ligand as significantly DE (i.e., |LFC|>1 for both but Padj<0.01 for only one of these). White cells indicate anti-regulation or no fold change at all in at least one of them.
Figure S3: functional interaction network between genes (ovals) and metabolites (diamonds) in the 'Purine catabolism' pathway in a) pancreatic and b) prostatic cancer. Red nodes indicate upregulated components, blue nodes indicate downregulated components, and

green nodes indicate no information available. The network shows that over-activation of the pathway is contributed by over-expression of both genes and metabolites.
Figure S4:Kaplan-Meier curve for survival analysis done by stratifying patients based on expression values of representative GPCR-ligand axes, found to be more significantly associated with lower survival than individual components in several cancer types.
Figure S5: Kaplan-Meier curve for survival analysis done by stratifying patients based on expression values of SSTR2-SST axis in either head and neck or adrenal gland cancers.
Figure S6:G protein coupling preferences of axes found significantly associated with higher survival in head and neck: i.e., *SSTR2-SST*, *RXFP3-INSL5* and *RXFP1-RLN3*
Figure S7: The bubble plot shows the correlation between the combined-expression levels of GPCR-ligand pairs and patient survival across cancer subtypes. The pairs with a log rank p-value <0.05 and also lower than log rank p-values for individual GPCR/ligand are displayed. Bubble color is proportional to HR: i.e., HR>1 : High expression is correlated with high survival (red); HR<1: High expression is correlated with poor survival (blue). Bubble diameters are proportional to the -log10(log-rank p-value). Green highlighted bubbles represent the most significant instances (sample sizes>5, FDR<0.1).
Figure S8: The bubble plot shows the correlation between the combined-expression levels of GPCR-enzyme pairs and patient survival across various subtypes. The pairs with a log rank p-value <0.05 and also lower than log rank p-values for individual GPCR/ligand are displayed. Bubble color is proportional to HR: i.e., HR>1 : High expression is correlated with high survival (red); HR<1: High expression is correlated with poor survival (blue). Bubble diameters are proportional to the -log10(log-rank p-value). Green highlighted bubbles represent the most significant instances (sample sizes>5, FDR<0.1).
Figure S9: number of Pubmed evidences obtained by querying with the following keywords: a) GPCR name *and* ligand name *and* cancer;b) GPCR name *and* ligand name *and* cancer *and* tissue; c) GPCR name *and* ligand name *and* cancer *and* immunotherapy; d) GPCR name *and* enzyme name *and* cancer

Supplementary Tables

Table S1: GPCR ligands in Reactome Pathways (Metabolism and Signal Transduction domains)
Table S2. List of GPCR ligands with cognate receptors and biosynthetic enzymes from RHEADB
Table S3. Tissue-wise sample distribution in the data retrieved from UCSCXena.
Table S4. reactome pathways enrichment scores (ES) and differential abundance scores (PAS) calculated from transcripts and metabolites log2fold changes
Table S5: GPCR based survival analysis - cancer tissue/TCGA molecular subtypes
Table S6: ligand based survival analysis - cancer tissue/TCGA molecular subtypes
Table S7: enzyme based survival analysis - cancer tissues/TCGA molecular subtypes
Table S8: GPCR-ligand based survival analysis - cancer tissues/TCGA molecular subtypes
Table S9: GPCR-enzyme based survival analysis - cancer tissues/TCGA molecular subtypes
Table S10: GPCR ligands activity from PRISM cancer cell line drug repurposing hub

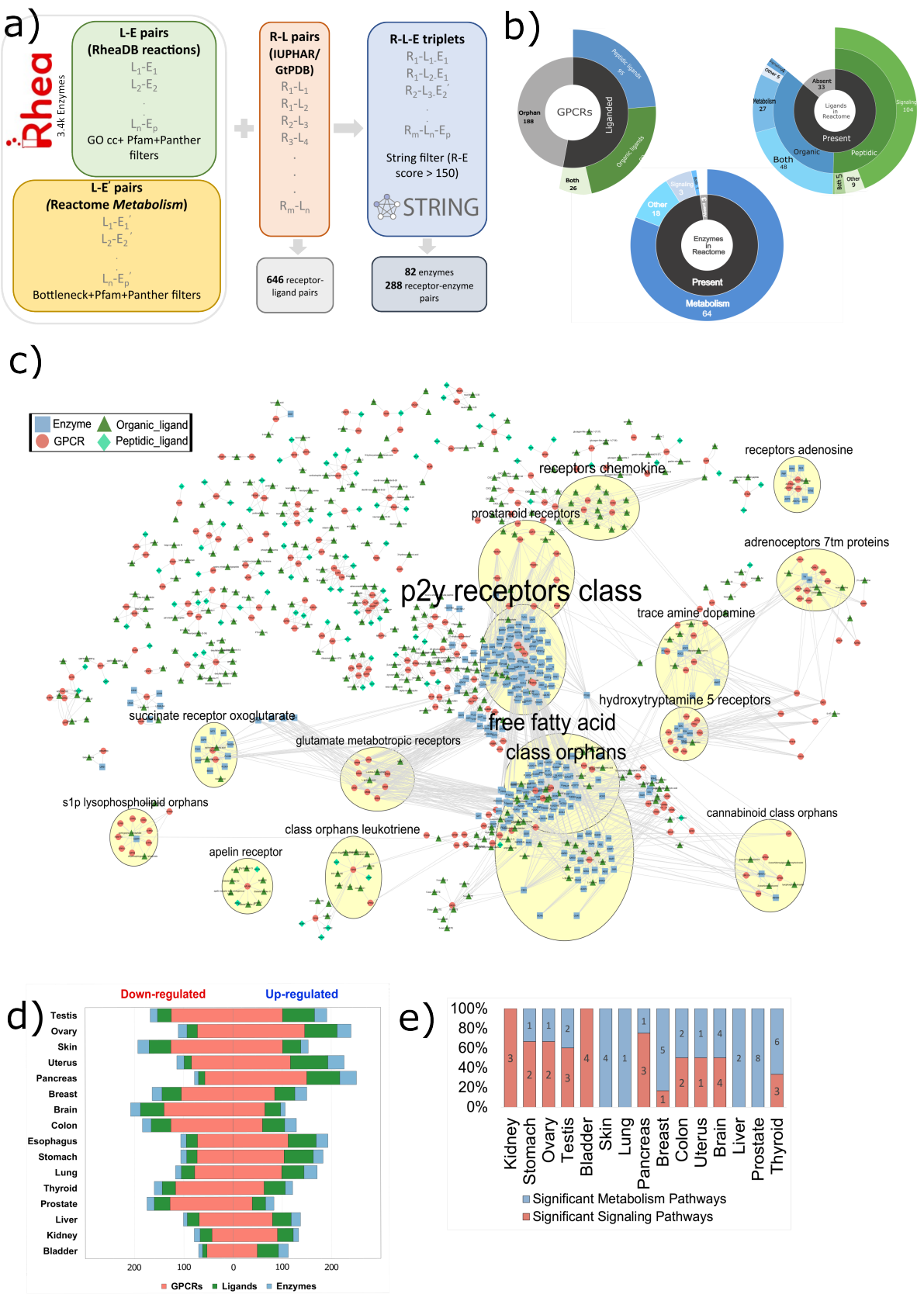
a)
Rhea
3.4k Enzymes
L-E pairs
(RheaDB reactions)
L1-E1
L2-E2
Ln-Ep
GO cc+ Pfam+Panther filters
L-E' pairs
(Reactome Metabolism)
L1-E1'
L2-E2'
Ln-Ep'
Bottleneck+Pfam+Panther filters
R-L pairs
(IUPHAR/ GtPDB)
R1-L1
R1-L2
R2-L3
R3-L4
Rm-Ln
646 receptor-ligand pairs
R-L-E triplets
R1-L1.E1
R1-L2.E1'
R2-L3.E2'
Rm-Ln-Ep
String filter (R-E score > 150)
STRING
82 enzymes
288 receptor-enzyme pairs
b)
GPCRs
Ligended
Orphan 188
Peptidic_ligands 85
Organic_ligands
Both 26
Ligands in Reactome
Present
Absent 33
Signaling 104
Peptidic
Organic
Both 48
Metabolism 27
Other 5
Both 9
Other 9
Signaling 3
Enzymes in Reactome
Present
Metabolism 64
Other 18
c)
Enzyme
GPCR
Organic_ligand
Peptidic_ligand
receptors chemokine
receptors adenosine
prostanoid receptors
adrenoceptors 7tm proteins
p2y receptors class
trace amine dopamine
hydroxytryptamine 5 receptors
succinate receptor oxoglutarate
glutamate metabotropic receptors
free fatty acid class orphans
s1p lysophospholipid orphans
class orphans leukotriene
apelin receptor
cannabinoid class orphans
d)
Down-regulated
Up-regulated
Testis
Ovary
Skin
Uterus
Pancreas
Breast
Brain
Colon
Esophagus
Stomach
Lung
Thyroid
Prostate
Liver
Kidney
Bladder
200
100
0
100
200
GPCRs
Ligands
Enzymes
e)
100%
80%
60%
40%
20%
0%
Kidney
Stomach
Ovary
Testis
Bladder
Skin
Lung
Pancreas
Breast
Colon
Uterus
Brain
Liver
Prostate
Thyroid
Significant Metabolism Pathways
Significant Signaling Pathways

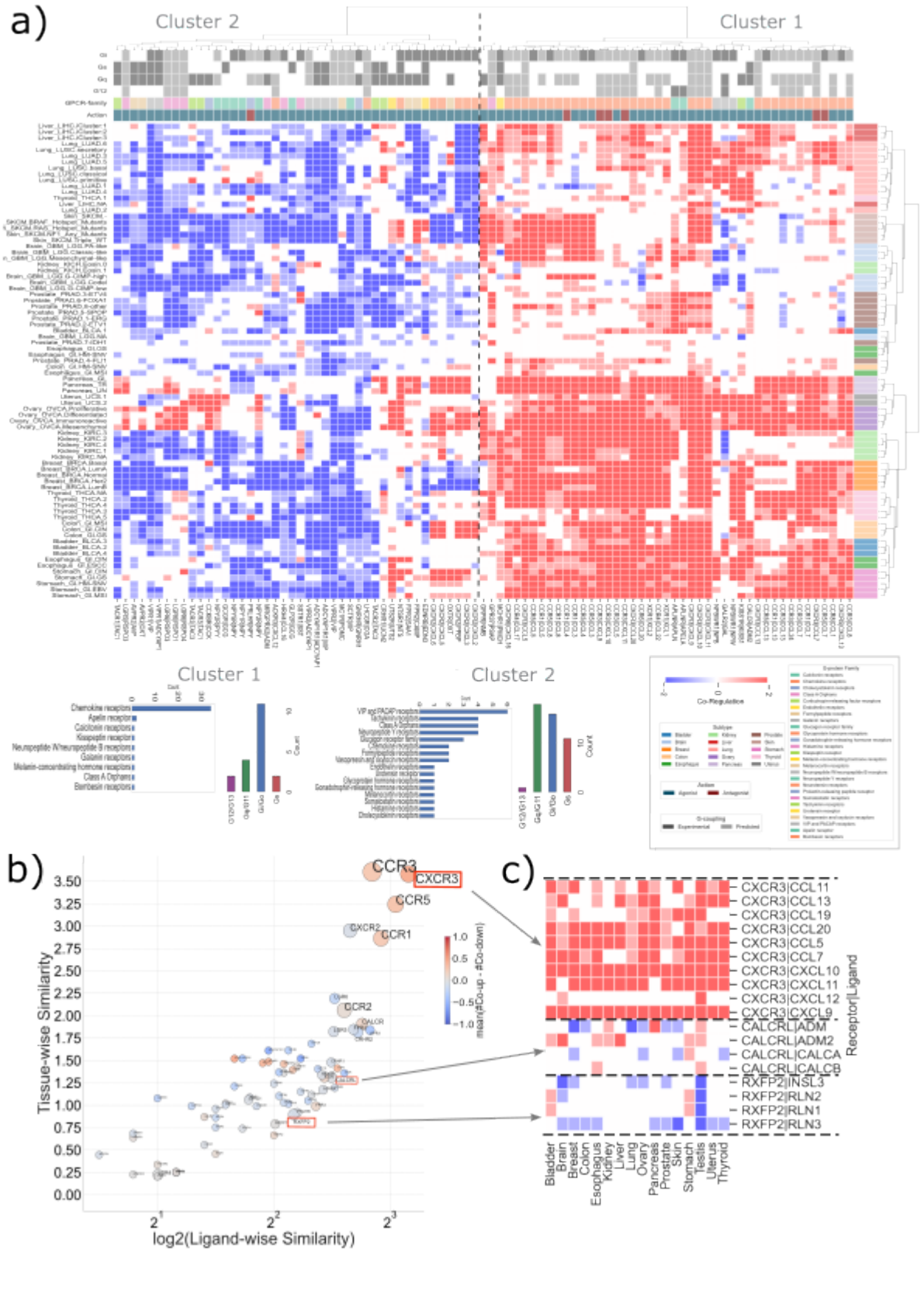
a)
Cluster 2
Cluster 1
Cluster 1
Cluster 2
b)
Tissue-wise Similarity
log2(Ligand-wise Similarity)
CCR3
CXCR3
CCR5
CXCR2
CCR1
CCR2
CALCR
RXFP2
mean(#Co-up - #Co-down)
c)
CXCR3|CCL11
CXCR3|CCL13
CXCR3|CCL19
CXCR3|CCL20
CXCR3|CCL5
CXCR3|CCL7
CXCR3|CXCL10
CXCR3|CXCL11
CXCR3|CXCL12
CXCR3|CXCL9
CALCRL|ADM
CALCRL|ADM2
CALCRL|CALCA
CALCRL|CALCB
RXFP2|INSL3
RXFP2|RLN2
RXFP2|RLN1
RXFP2|RLN3
Receptor|Ligand
Bladder
Brain
Breast
Colon
Esophagus
Kidney
Liver
Lung
Ovary
Pancreas
Prostate
Skin
Stomach
Testis
Uterus
Thyroid

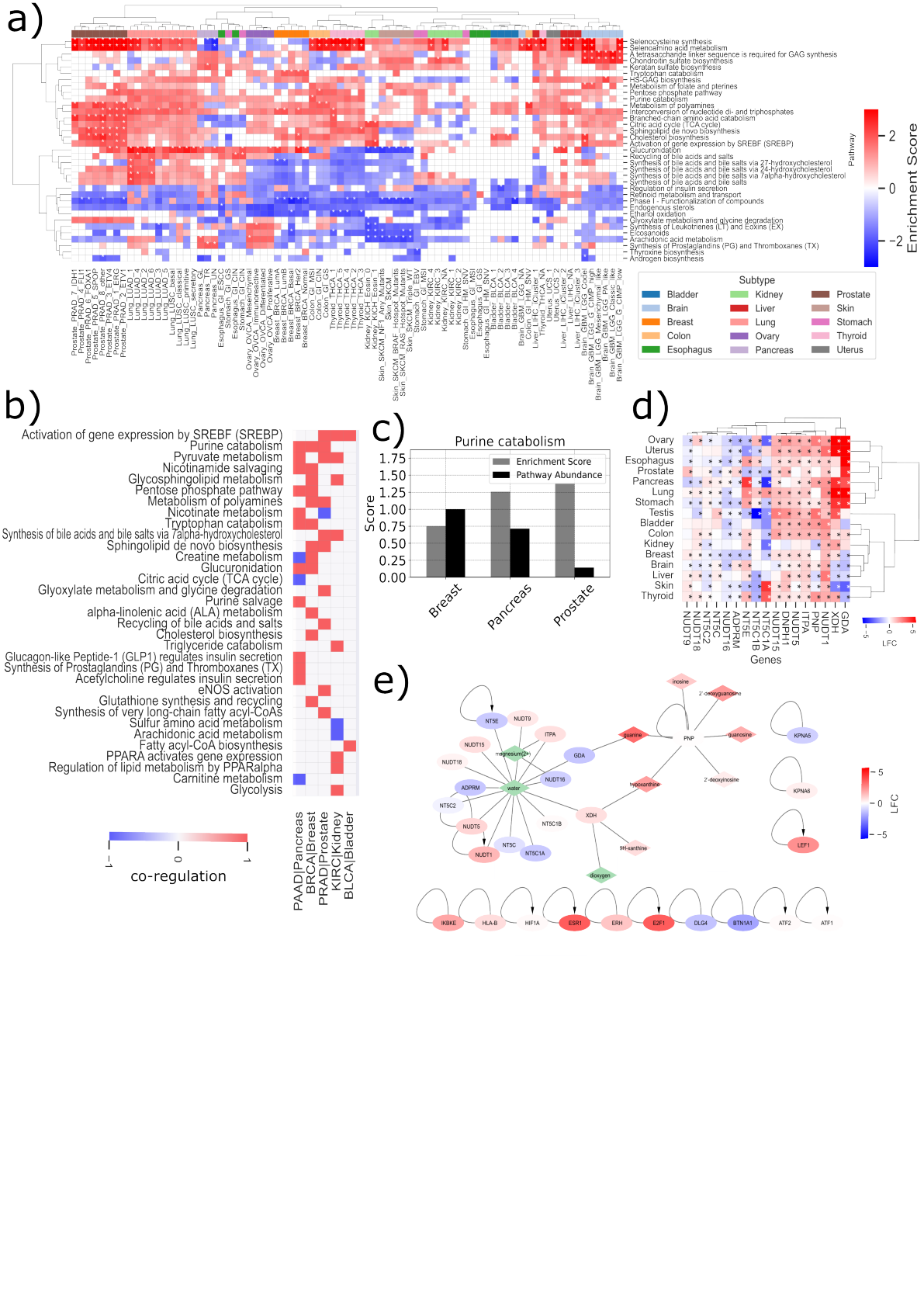
a)
Selenocysteine synthesis
Selenoamino acid metabolism
A tetrasaccharide linker sequence is required for GAG synthesis
Chondroitin sulfate biosynthesis
Keratan sulfate biosynthesis
Tryptophan catabolism
HS-GAG biosynthesis
Metabolism of folate and pterines
Pentose phosphate pathway
Purine catabolism
Metabolism of polyamines
Interconversion of nucleotide di- and triphosphates
Branched-chain amino acid catabolism
Citric acid cycle (TCA cycle)
Sphingolipid de novo biosynthesis
Cholesterol biosynthesis
Activation of gene expression by SREBF (SREBP)
Glucuronidation
Recycling of bile acids and salts
Synthesis of bile acids and bile salts via 27-hydroxycholesterol
Synthesis of bile acids and bile salts via 24-hydroxycholesterol
Synthesis of bile acids and bile salts via 7alpha-hydroxycholesterol
Synthesis of bile acids and bile salts
Regulation of insulin secretion
Retinoid metabolism and transport
Phase I - Functionalization of compounds
Endogenous sterols
Ethanol oxidation
Glyoxylate metabolism and glycine degradation
Synthesis of Leukotrienes (LT) and Eoxins (EX)
Eicosanoids
Arachidonic acid metabolism
Synthesis of Prostaglandins (PG) and Thromboxanes (TX)
Thyroxine biosynthesis
Androgen biosynthesis
Pathway
Enrichment Score
2
0
−2
Subtype
Bladder
Brain
Breast
Colon
Esophagus
Kidney
Liver
Lung
Ovary
Pancreas
Prostate
Skin
Stomach
Thyroid
Uterus
b)
Activation of gene expression by SREBF (SREBP)
Purine catabolism
Pyruvate metabolism
Nicotinamide salvaging
Glycosphingolipid metabolism
Pentose phosphate pathway
Metabolism of polyamines
Nicotinate metabolism
Tryptophan catabolism
Synthesis of bile acids and bile salts via 7alpha-hydroxycholesterol
Sphingolipid de novo biosynthesis
Creatine metabolism
Glucuronidation
Citric acid cycle (TCA cycle)
Glyoxylate metabolism and glycine degradation
Purine salvage
alpha-linolenic acid (ALA) metabolism
Recycling of bile acids and salts
Cholesterol biosynthesis
Triglyceride catabolism
Glucagon-like Peptide-1 (GLP1) regulates insulin secretion
Synthesis of Prostaglandins (PG) and Thromboxanes (TX)
Acetylcholine regulates insulin secretion
eNOS activation
Glutathione synthesis and recycling
Synthesis of very long-chain fatty acyl-CoAs
Sulfur amino acid metabolism
Arachidonic acid metabolism
Fatty acyl-CoA biosynthesis
PPARA activates gene expression
Regulation of lipid metabolism by PPARalpha
Carnitine metabolism
Glycolysis
PAAD|Pancreas
BRCA|Breast
PRAD|Prostate
KIRC|Kidney
BLCA|Bladder
co-regulation
−1
0
1
c)
Purine catabolism
Enrichment Score
Pathway Abundance
Score
1.75
1.50
1.25
1.00
0.75
0.50
0.25
0.00
Breast
Pancreas
Prostate
d)
Ovary
Uterus
Esophagus
Prostate
Pancreas
Lung
Stomach
Testis
Bladder
Colon
Kidney
Breast
Brain
Liver
Skin
Thyroid
NUDT9
NUDT18
NT5C2
NUDT16
ADPRM
NT5E
NT5C1A
NT5C1B
NUDT15
DNPH1
NUDT5
ITPA
PNP
NUDT1
XDH
GDA
Genes
LFC
−5
0
5
e)
inosine
2' deoxyguanosine
guanine
PNP
guanosine
2' deoxyinosine
hypoxanthine
NT5E
NUDT9
ITPA
NUDT15
magnesium(2+)
GDA
NUDT18
ADPRM
water
NUDT16
NT5C2
NUDT5
NT5C1B
XDH
NUDT1
NT5C
NT5C1A
9H-xanthine
dioxygen
KPNA5
KPNA6
LEF1
LFC
5
0
−5
IKBKE
HLA-B
HIF1A
ESR1
ERH
E2F1
DLG4
BTN1A1
ATF2
ATF1

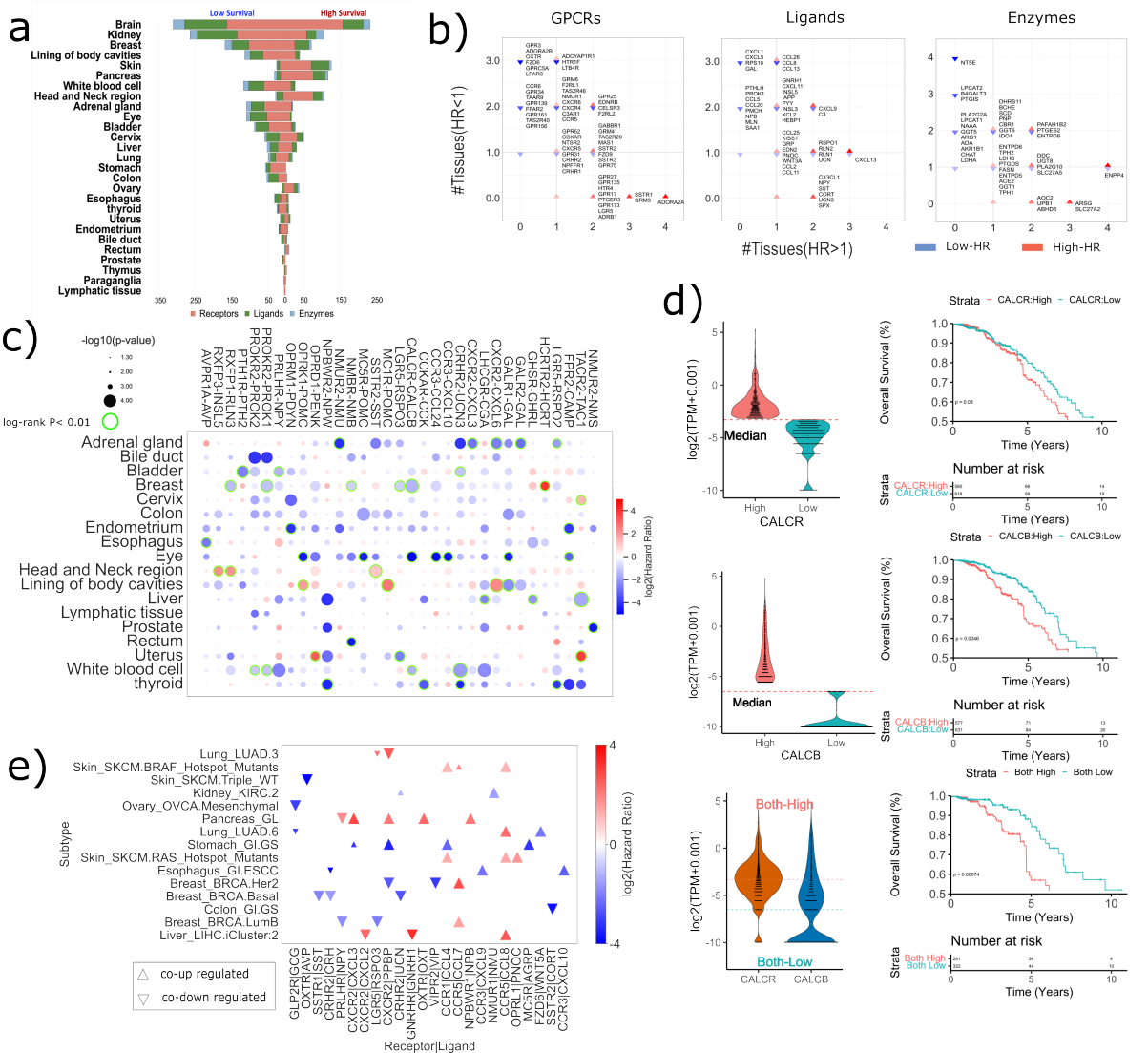
a
Low Survival
High Survival
Brain
Kidney
Breast
Lining of body cavities
Skin
Pancreas
White blood cell
Head and Neck region
Adrenal gland
Eye
Bladder
Cervix
Liver
Lung
Stomach
Colon
Ovary
Esophagus
thyroid
Uterus
Endometrium
Bile duct
Rectum
Prostate
Thymus
Paraganglia
Lymphatic tissue
Receptors
Ligands
Enzymes
b)
GPCRs
Ligands
Enzymes
#Tissues(HR<1)
#Tissues(HR>1)
Low-HR
High-HR
c)
-log10(p-value)
log-rank P< 0.01
log2(Hazard Ratio)
d)
Median
CALCR
CALCB
Both-High
Both-Low
log2(TPM+0.001)
Strata
Overall Survival (%)
Time (Years)
Number at risk
e)
Subtype
Lung_LUAD.3
Skin_SKCM.BRAF_Hotspot_Mutants
Skin_SKCM.Triple_WT
Kidney_KIRC.2
Ovary_OVCA.Mesenchymal
Pancreas_GI
Lung_LUAD.6
Stomach_GI.GS
Skin_SKCM.RAS_Hotspot_Mutants
Esophagus_GI.ESCC
Breast_BRCA.Her2
Breast_BRCA.Basal
Colon_GI.GS
Breast_BRCA.LumB
Liver_LIHC.iCluster:2
log2(Hazard Ratio)
co-up regulated
co-down regulated
Receptor|Ligand

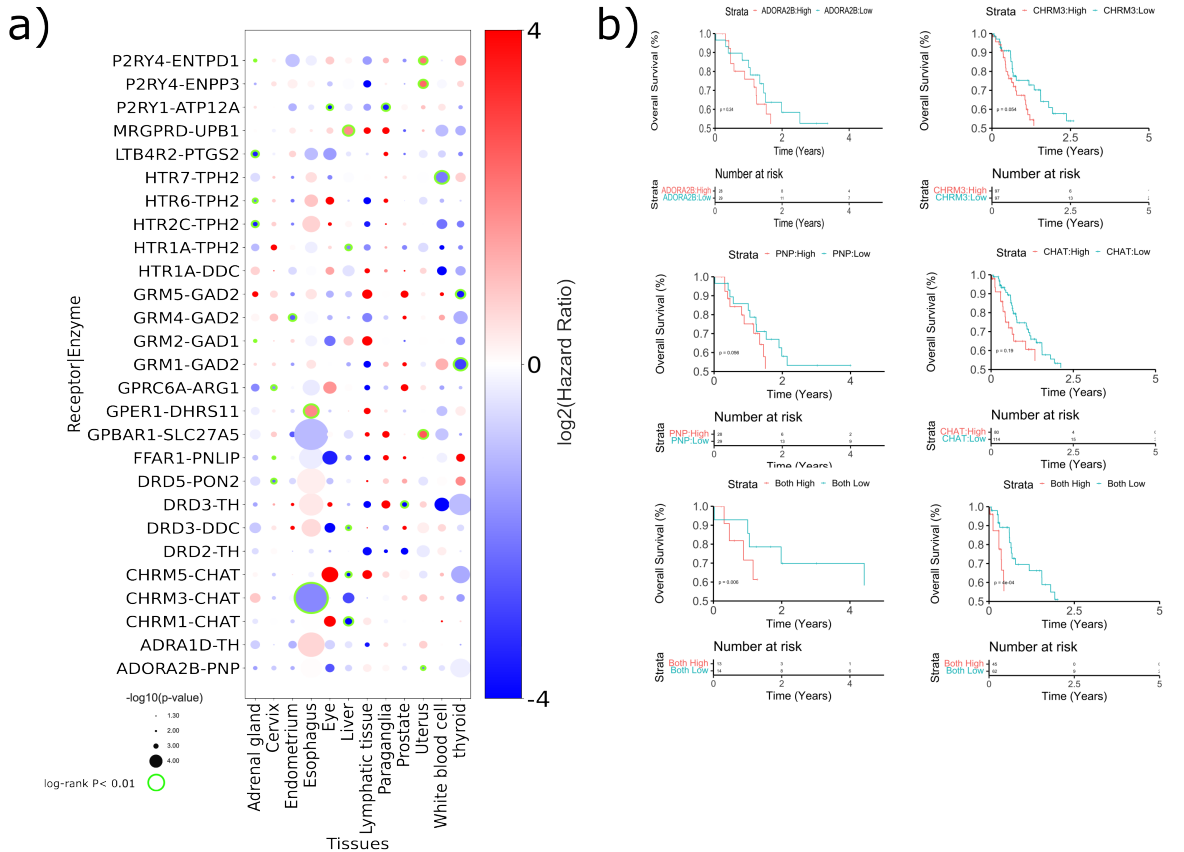
a)
P2RY4-ENTPD1
P2RY4-ENPP3
P2RY1-ATP12A
MRGPRD-UPB1
LTB4R2-PTGS2
HTR7-TPH2
HTR6-TPH2
HTR2C-TPH2
HTR1A-TPH2
HTR1A-DDC
GRM5-GAD2
GRM4-GAD2
GRM2-GAD1
GRM1-GAD2
GPRC6A-ARG1
GPER1-DHRS11
GPBAR1-SLC27A5
FFAR1-PNLIP
DRD5-PON2
DRD3-TH
DRD3-DDC
DRD2-TH
CHRM5-CHAT
CHRM3-CHAT
CHRM1-CHAT
ADRA1D-TH
ADORA2B-PNP
Receptor|Enzyme
Adrenal gland
Cervix
Endometrium
Esophagus
Eye
Liver
Lymphatic tissue
Paraganglia
Prostate
Uterus
White blood cell
thyroid
Tissues
log2(Hazard Ratio)
4
0
-4
-log10(p-value)
1.30
2.00
3.00
4.00
log-rank P< 0.01
b)
Strata - ADORA2B:High - ADORA2B:Low
Strata - CHRM3:High - CHRM3:Low
Strata - PNP:High - PNP:Low
Strata - CHAT:High - CHAT:Low
Strata - Both High - Both Low
Overall Survival (%)
Time (Years)
Number at risk
Strata

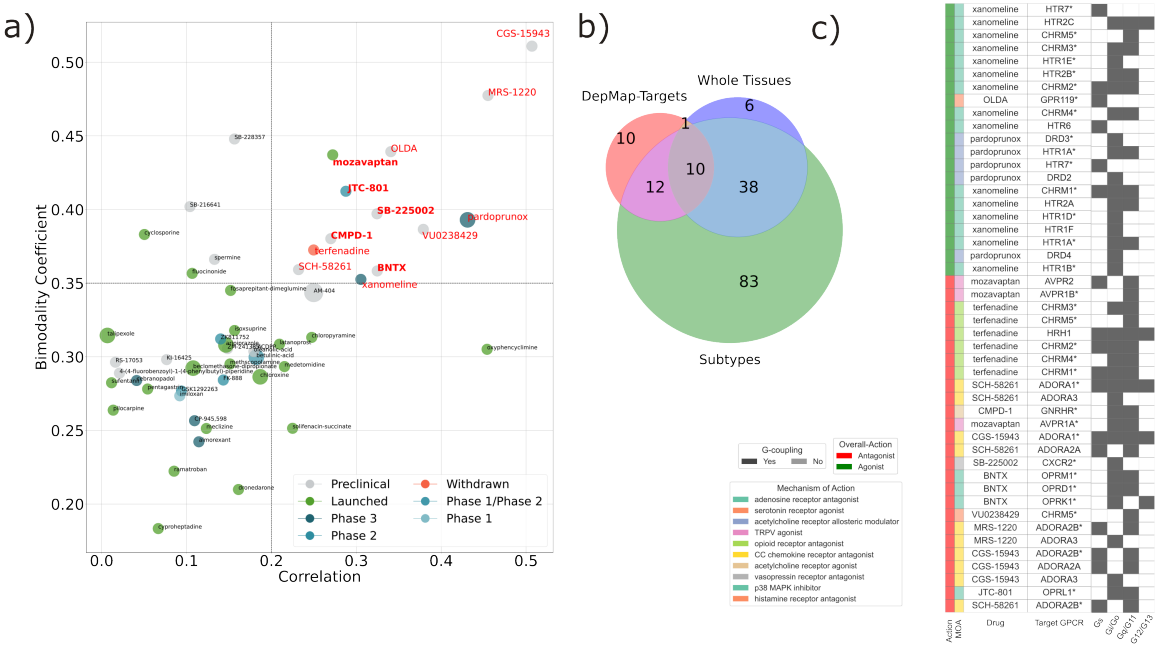
a)
b)
c)
Bimodality Coefficient
Correlation
CGS-15943
MRS-1220
OLDA
mozavaptan
JTC-801
SB-225002
pardoprunox
VU0238429
CMPD-1
terfenadine
SCH-58261
BNTX
xanomeline
Preclinical
Launched
Phase 3
Phase 2
Withdrawn
Phase 1/Phase 2
Phase 1
DepMap-Targets
Whole Tissues
Subtypes
G-coupling
Yes
No
Overall-Action
Antagonist
Agonist
Mechanism of Action
adenosine receptor antagonist
serotonin receptor agonist
acetylcholine receptor allosteric modulator
TRPV agonist
opioid receptor antagonist
CC chemokine receptor antagonist
acetylcholine receptor agonist
vasopressin receptor antagonist
p38 MAPK inhibitor
histamine receptor antagonist
Action
MOA
Drug
Target GPCR
Gs
Gi/Go
Gq/G11
G12/G13

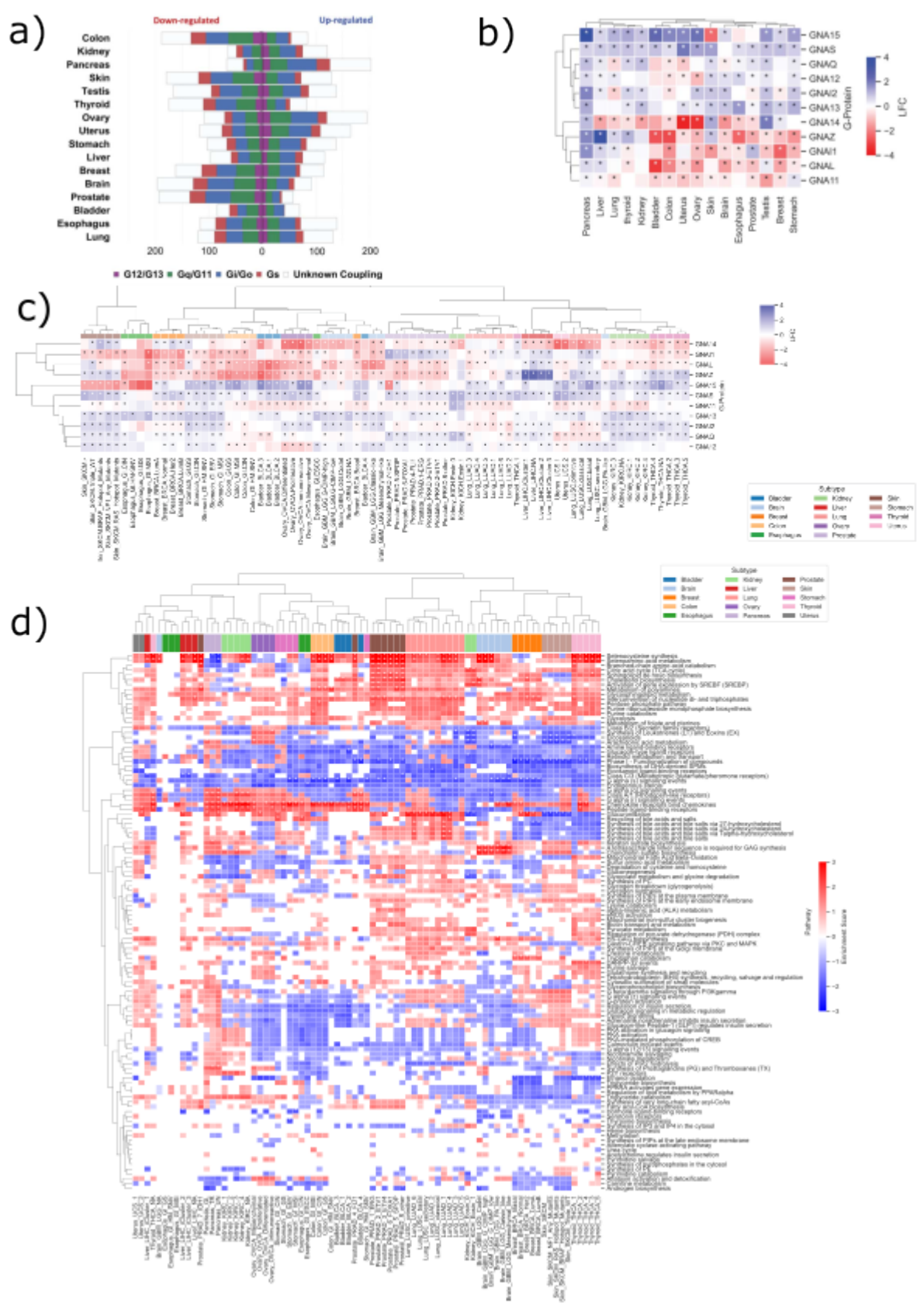
a)
Down-regulated
Up-regulated
Colon
Kidney
Pancreas
Skin
Testis
Thyroid
Ovary
Uterus
Stomach
Liver
Breast
Brain
Prostate
Bladder
Esophagus
Lung
200
100
0
100
200
G12/G13
Gq/G11
Gi/Go
Gs
Unknown Coupling
b)
GNA15
GNAS
GNAQ
GNA12
GNAI2
GNA13
GNA14
GNAZ
GNAI1
GNAL
GNA11
G-Protein
LFC
Pancreas
Liver
Lung
Thyroid
Kidney
Bladder
Colon
Uterus
Ovary
Skin
Brain
Esophagus
Prostate
Testis
Breast
Stomach
c)
Subtype
d)
Subtype
Pathway
Enrichment Score

G-coupling
Experimental
Predicted
Action
Agonist
Antagonist
Unknown
G-protein Family
Angiotensin receptors
Bradykinin receptors
Calcitonin receptors
Chemokine receptors
Cholecystokinin receptors
Class A Orphans
Corticotropin-releasing factor receptors
Endothelin receptors
Formylpeptide receptors
Class Frizzled GPCRs
Galanin receptors
Ghrelin receptor
Glucagon receptor family
Glycoprotein hormone receptors
Gonadotrophin-releasing hormone receptors
Histamine receptors
Chemerin receptors
Kisspeptin receptor
Melanin-concentrating hormone receptors
Melanocortin receptors
Motilin receptor
Neuromedin U receptors
Neuropeptide FF/neuropeptide AF receptors
Neuropeptide W/neuropeptide B receptors
Neuropeptide Y receptors
Neurotensin receptors
Complement peptide receptors
Opioid receptors
Orexin receptors
Parathyroid hormone receptors
QRFP receptor
Prokineticin receptors
Prolactin-releasing peptide receptor
Relaxin family peptide receptors
Somatostatin receptors
Tachykinin receptors
Urotensin receptor
Vasopressin and oxytocin receptors
VIP and PACAP receptors
Apelin receptor
Bombesin receptors
Subtype
Bladder
Brain
Breast
Colon
Esophagus
Kidney
Liver
Lung
Ovary
Pancreas
Prostate
Skin
Stomach
Thyroid
Uterus
Gi
Gs
Gq
G12
GPCR-family
Action
Co-Regulation
2
0
−2
Receptor|Ligand
CCR5|CCL3
CCR5|CCL4
CCR1|CCL3
CCR1|CCL4
CCR1|CCL8
CCR5|CCL8
CCR1|CCL5
CCR5|CCL5
CXCR3|CCL5
CCR4|CCL17
CXCR6|CXCL16
CXCR3|CXCL11
CXCR3|CXCL10
CXCR3|CXCL9
APLNR|APELA
APLNR|APLN
XCR1|XCL1
CCR4|CCL22
XCR1|XCL2
CCR6|CCL20
CXCR3|CCL20
CCR3|CXCL11
CCR3|CCL5
CCR3|CXCL10
CCR3|CXCL9
GALR2|GAL
GALR3|GAL
MCHR2|PMCH
NPBWR1|NPB
CALCR|CALCA
CALCR|CALCB
CALCR|ADM2
KISS1R|KISS1
NPBWR1|NPW
FZD6|WNT4
FZD6|WNT5A
CCR3|CCL28
PTH2R|PTHLH
CALCR|IAPP
ACKR3|CXCL11
CCR2|CCL13
CCR2|CCL24
CCR2|CCL11
CCR2|CCL8
CCR5|CCL11
CXCR3|CCL11
CCR2|CCL7
CCR3|CCL11
GRPR|GRP
GRPR|NMB
MCHR1|PMCH
CCR6|DEFB4A
FPR3|MT-RNR2
OPRL1|PNOC
GPR37|PSAP
GPR37L1|PSAP
FPR3|HEBP1
CCR9|CCL25
MC5R|AGRP
NMUR2|NMU
CCR1|CCL15
CCR3|CCL15
CCR3|CCL24
CCR3|CCL26
CCR3|CCL13
CCR1|CCL13
CCR5|CCL13
CXCR3|CCL13
CCR3|CCL8
CXCR5|CXCL13
CCR8|CCL1
CCR5|CCL7
CXCR3|CCL7
CCR1|CCL7
CCR3|CCL7
TSHR|CGA
PRLHR|PTHLH
PTH1R|PTHLH
QRFPR|QRFP
CALCRL|CALCA
GALR1|GAL
RXFP1|RLN2
RXFP1|RLN1
CCR2|CCL26
CCR1|CCL23
CCR1|CCL14
CCR5|CCL14
NMUR1|NMU
NMBR|NMB
CALCRL|CALCB
RXFP2|RLN2
RXFP2|RLN1
CCR5|CCL16
CXCR3|CXCL12
MLNR|MLN
CXCR4|CXCL12
GHSR|GHRL
C5AR1|C5
C5AR1|RPS19
LGR4|RSPO1
LGR4|RSPO4
LGR4|RSPO2
LGR4|RSPO3
CCKBR|GAST
FZD6|WNT3A
SCTR|SCT
NPY5R|PPY
GHRHR|GHRH
NMUR2|NMS
PROKR2|PROK1
PROKR2|PROK2
RXFP4|INSL5
RXFP4|RLN3
NPBWR2|NPB
OPRD1|PDYN
RXFP3|INSL5
NPBWR2|NPW
RXFP3|RLN3
CCR7|CCL21
CCRL2|CCL19
CCR7|CCL19
CXCR3|CCL19
FPR2|CAMP
FPR2|MT-RNR2
ACKR4|CCL19
ACKR4|CCL21
FPR2|SAA1
CXCR2|CXCL8
CXCR1|CXCL6
CXCR1|CXCL8
GPR1|RARRES2
CALCR|ADM
EDNRA|EDN1
EDNRA|EDN2
CALCRL|ADM
FPR2|ANXA1
CX3CR1|CX3CL1
FPR3|ANXA1
C3AR1|C3
CCR2|CCL2
CCR3|CCL2
CCR5|CCL2
CALCRL|ADM2
ACKR4|CCL25
GPR75|CCL5
FSHR|CGA
LHCGR|CGA
GNRHR|GNRH1
GNRHR|GNRH2
SCTR|VIP
MC1R|POMC
EDNRB|EDN3
RXFP1|RLN3
RXFP2|RLN3
AGTR1|AGT
AGTR2|AGT
CCR2|CCL16
CMKLR1|RARRES2
CRHR2|CRH
CRHR2|UCN3
MRGPRX1|PENK
OPRM1|PENK
CRHR1|CRH
CRHR1|UCN
CRHR2|UCN
C5AR2|C5
GLP1R|GCG
PRLHR|PRLH
AVPR2|OXT
AVPR2|AVP
CCR10|CCL27
RXFP2|INSL3
CCR10|CCL28
UTS2R|UTS2B
NMUR1|NMS
PTH1R|PTH2
HCRTR1|HCRT
VIPR1|GHRH
MC4R|AGRP
NPFFR2|NPFF
NPFFR1|NPVF
NPFFR1|NPFF
MC3R|AGRP
HCRTR2|HCRT
NTSR1|NTS
UTS2R|UTS2
TACR2|TAC1
TACR2|TAC3
SSTR2|SST
SSTR4|SST
SSTR2|CORT
SSTR4|CORT
SSTR3|CORT
SSTR3|SST
CRHR1|UCN2
CRHR2|UCN2
NTSR2|NTS
OPRK1|POMC
OPRD1|PENK
OPRD1|POMC
MC5R|POMC
MC3R|POMC
MC4R|POMC
NPY2R|NPY
PRLHR|NPY
NPY1R|NPY
NPY5R|NPY
TACR3|TAC1
TACR3|TAC3
GCGR|GCG
NPY1R|PYY
NPY2R|PYY
BDKRB1|KNG1
BDKRB2|KNG1
SSTR5|SST
GIPR|GIP
SSTR5|CORT
AVPR1A|OXT
AVPR1A|AVP
OXTR|OXT
OXTR|AVP
AVPR1B|OXT
AVPR1B|AVP
CCKAR|CCK
CCKBR|CCK
PROKR1|PROK1
PROKR1|PROK2
OPRK1|PDYN
OPRM1|PDYN
GALR2|SPX
GALR3|SPX
SSTR1|CORT
SSTR1|SST
NPY4R|NPY
NPY4R|PPY
NPY4R|PYY
VIPR2|VIP
ADCYAP1R1|VIP
ADCYAP1R1|ADCYAP1
VIPR2|ADCYAP1
VIPR1|ADCYAP1
VIPR1|VIP
GLP2R|GCG
HRH4|CCL16
TACR1|TAC1
TACR1|TAC3
ACKR3|CXCL12
MRGPRX2|ADM
CXCR2|CXCL5
CXCR2|CXCL1
CXCR2|CXCL6
CXCR2|CXCL2
CXCR2|CXCL3
CXCR2|PPBP
LGR5|RSPO2
LGR6|RSPO2
LGR6|RSPO4
LGR6|RSPO1
LGR6|RSPO3
LGR5|RSPO4
LGR5|RSPO1
LGR5|RSPO3
Uterus_UCS.1
Uterus_UCS.2
Ovary_OVCA.Proliferative
Ovary_OVCA.Mesenchymal
Ovary_OVCA.Differentiated
Ovary_OVCA.Immunoreactive
Pancreas_UN
Pancreas_GL
Pancreas_TR
Colon_GI.MSI
Colon_GI.CIN
Colon_GI.GS
Stomach_GI.EBV
Stomach_GI.HM-SNV
Stomach_GI.MSI
Stomach_GI.CIN
Stomach_GI.GS
Esophagus_GI.CIN
Esophagus_GI.ESCC
Bladder_BLCA.2
Bladder_BLCA.4
Bladder_BLCA.1
Bladder_BLCA.3
Kidney_KIRC.3
Kidney_KIRC.2
Kidney_KIRC.4
Kidney_KIRC.1
Kidney_KIRC.NA
Breast_BRCA.Basal
Breast_BRCA.Her2
Breast_BRCA.Normal
Breast_BRCA.LumA
Breast_BRCA.LumB
Thyroid_THCA.NA
Thyroid_THCA.4
Thyroid_THCA.2
Thyroid_THCA.1
Thyroid_THCA.3
Thyroid_THCA.5
Prostate_PRAD.3-ETV4
Prostate_PRAD.6-FOXA1
Prostate_PRAD.1-ERG
Prostate_PRAD.8-other
Prostate_PRAD.2-ETV1
Prostate_PRAD.5-SPOP
Kidney_KICH.Eosin.0
Kidney_KICH.Eosin.1
Prostate_PRAD.4-FLI1
Prostate_PRAD.7-IDH1
Brain_GBM_LGG.NA
Esophagus_GI.GS
Esophagus_GI.HM-SNV
Colon_GI.HM-SNV
Esophagus_GI.MSI
Liver_LIHC.iCluster:2
Liver_LIHC.iCluster:3
Liver_LIHC.NA
Liver_LIHC.iCluster:1
Lung_LUSC.basal
Lung_LUAD.2
Lung_LUSC.classical
Lung_LUAD.6
Lung_LUSC.primitive
Lung_LUSC.secretory
Lung_LUAD.1
Lung_LUAD.5
Lung_LUAD.3
Lung_LUAD.4
Skin_SKCM.-
Skin_SKCM.NF1_Any_Mutants
Skin_SKCM.BRAF_Hotspot_Mutants
Skin_SKCM.RAS_Hotspot_Mutants
Skin_SKCM.Triple_WT
Brain_GBM_LGG.CIMP-low
Brain_GBM_LGG.G-CIMP-high
Brain_GBM_LGG.PA-like
Brain_GBM_LGG.Classic-like
Brain_GBM_LGG.Mesenchymal-like

Pancreas

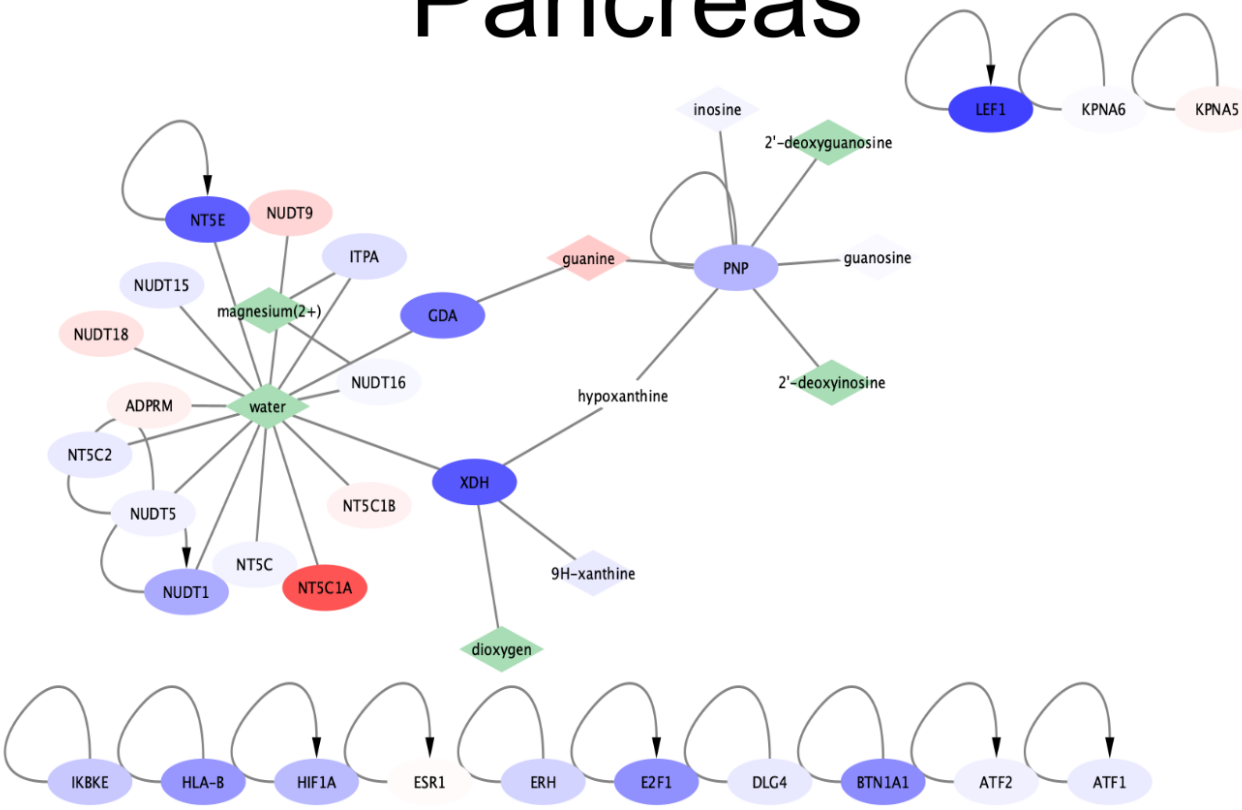

Prostate

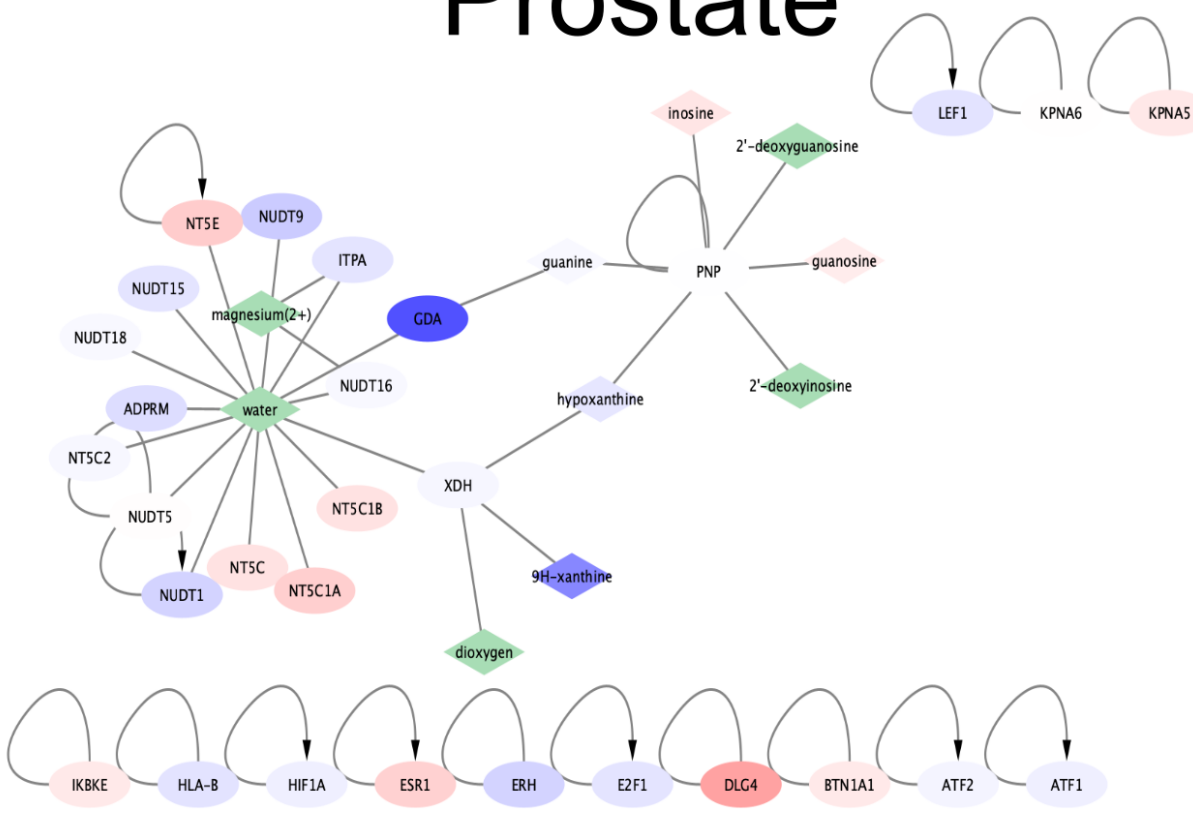

a)

CALCR-CALCB Eye

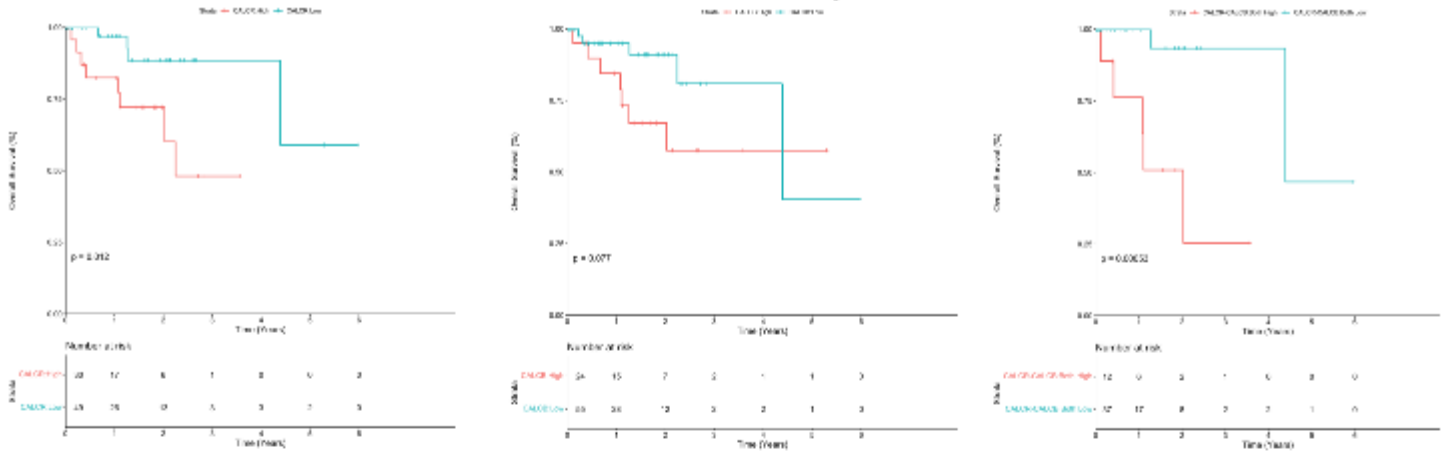

b)

NPBWR2-NPW Thyroid

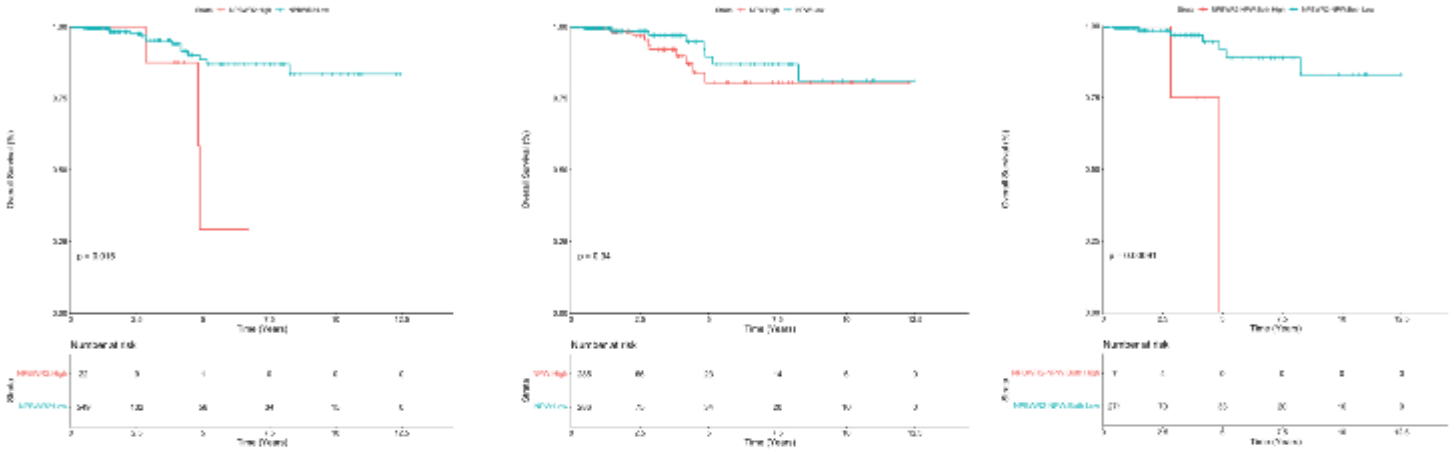

c)

CRHR2-UCN3 white blood cell

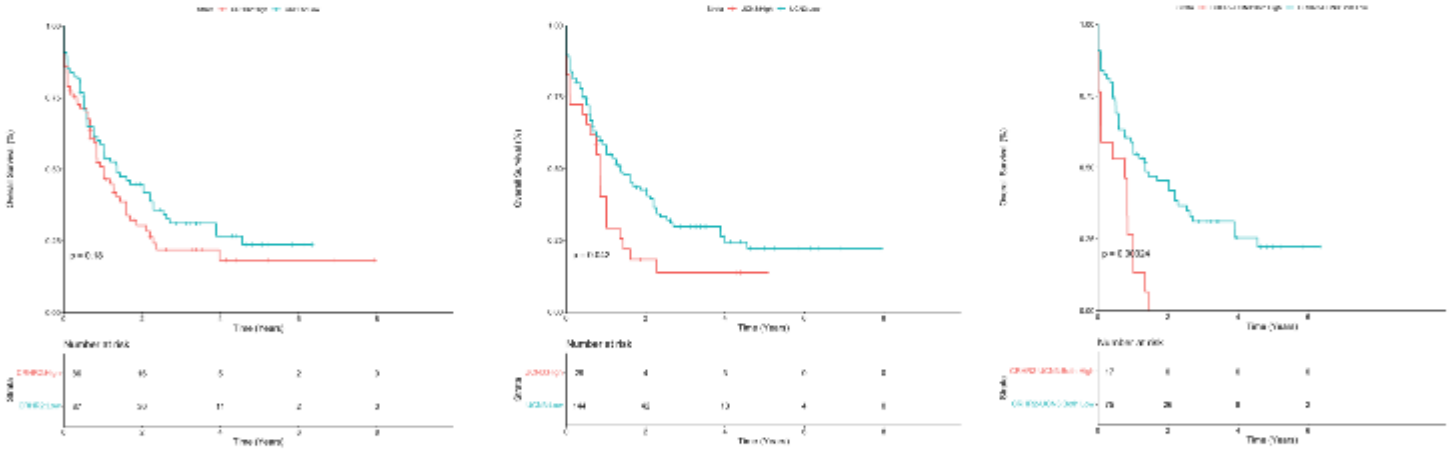

d)

PRLHR-NPY bladder

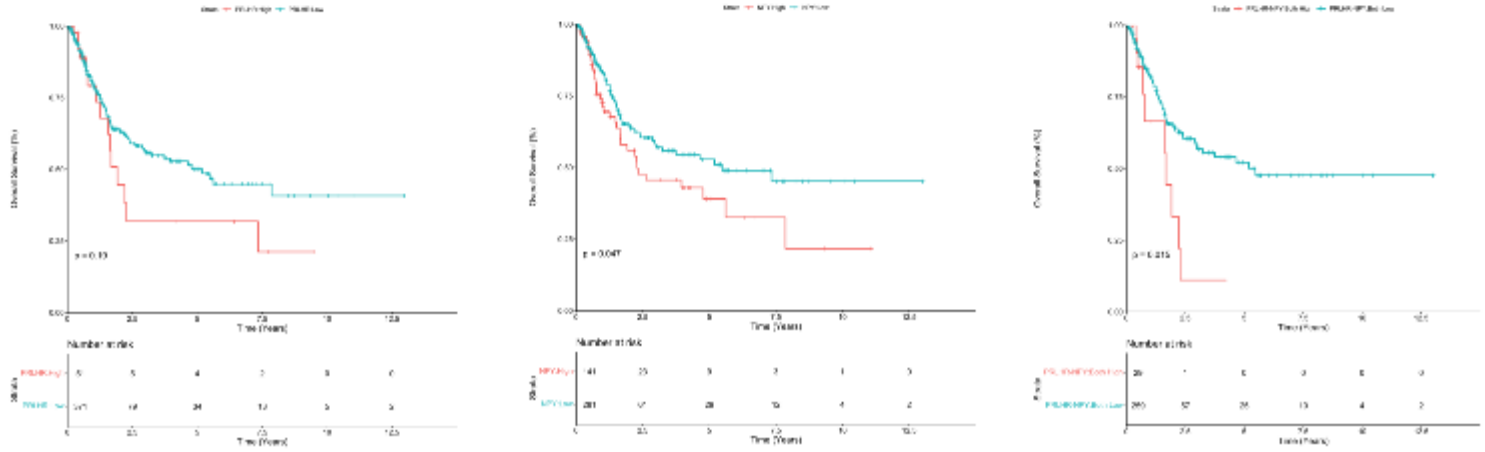

a)

SSTR2-SST head and neck

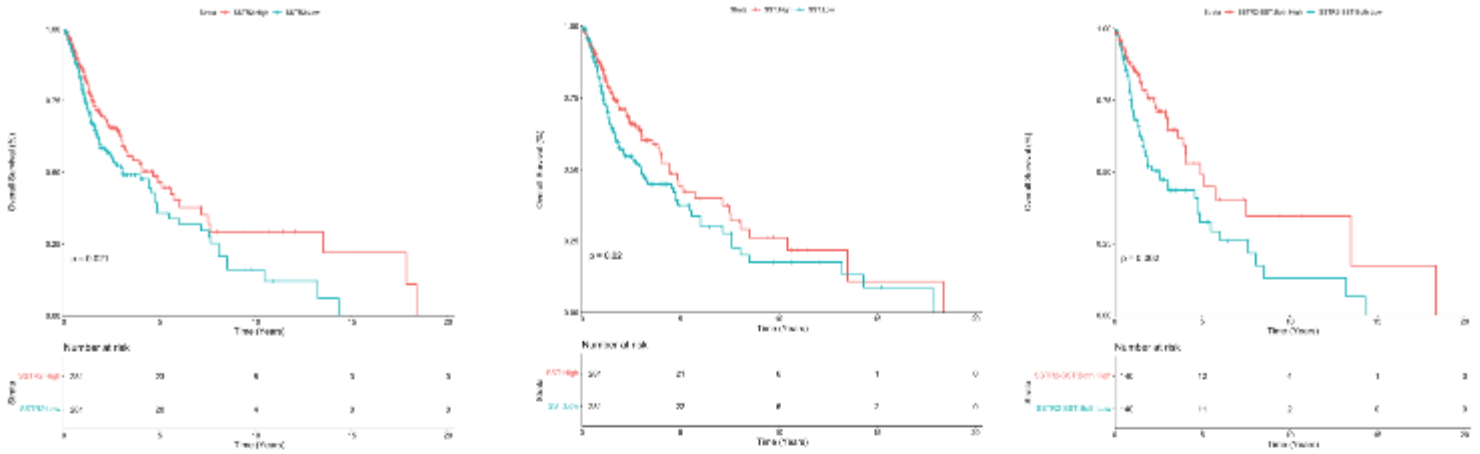

SSTR2-SST adrenal gland

b)

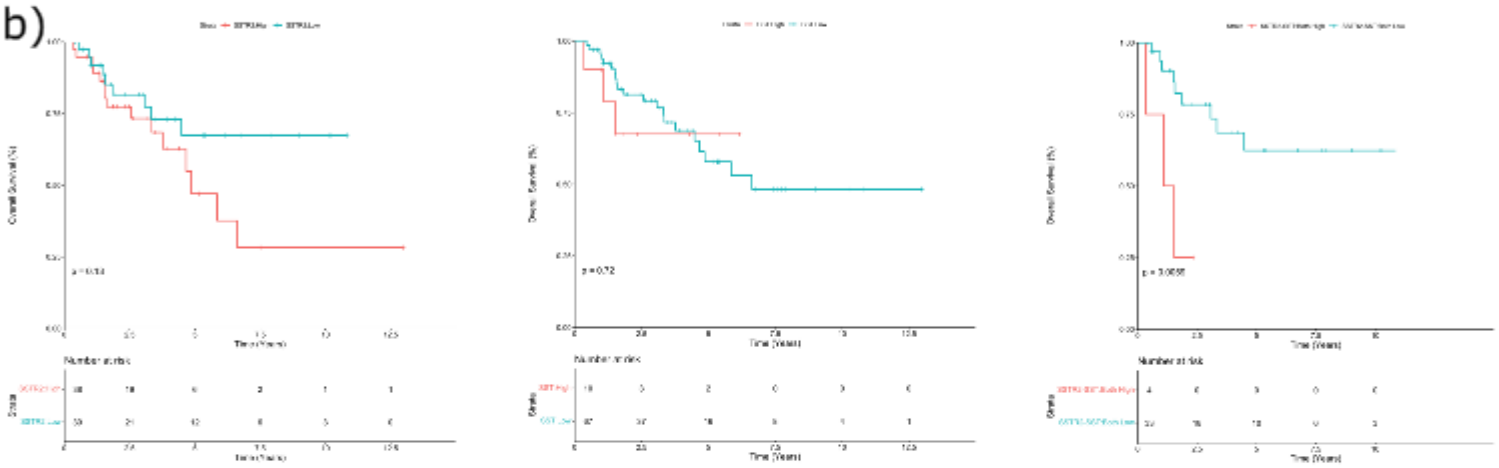

a)

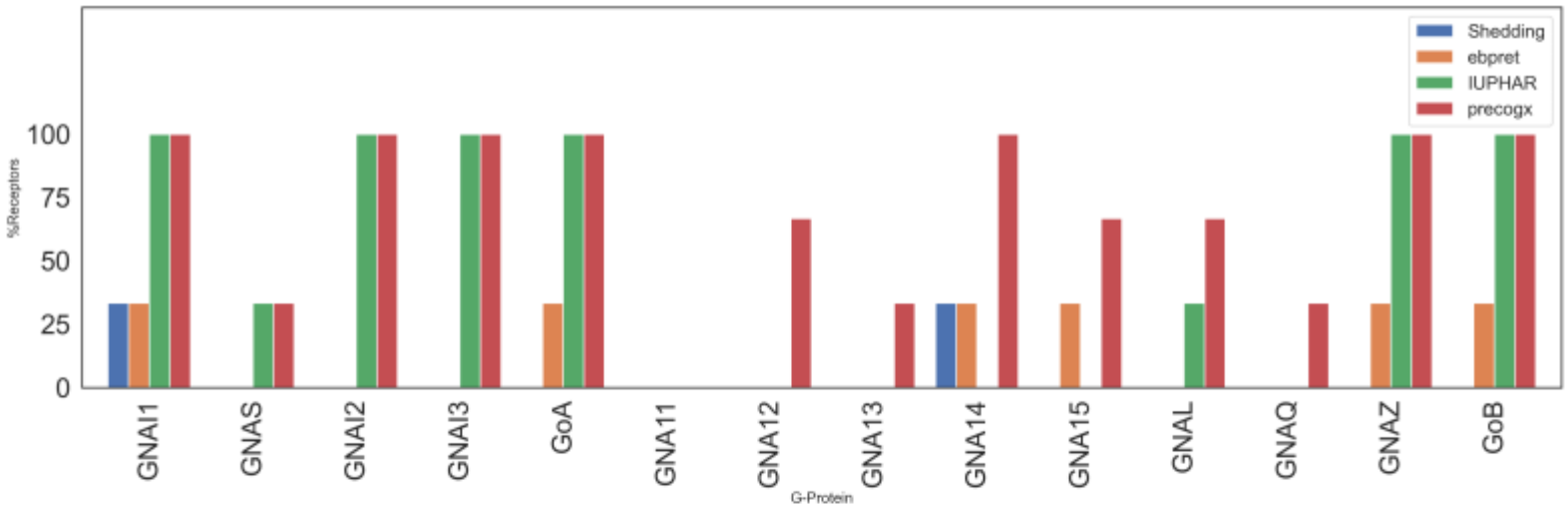
Shedding
ebpret
IUPHAR
precogx
%Receptors
100
75
50
25
0
GNAI1
GNAS
GNAI2
GNAI3
GoA
GNA11
GNA12
GNA13
GNA14
GNA15
GNAL
GNAQ
GNAZ
GoB
G-Protein

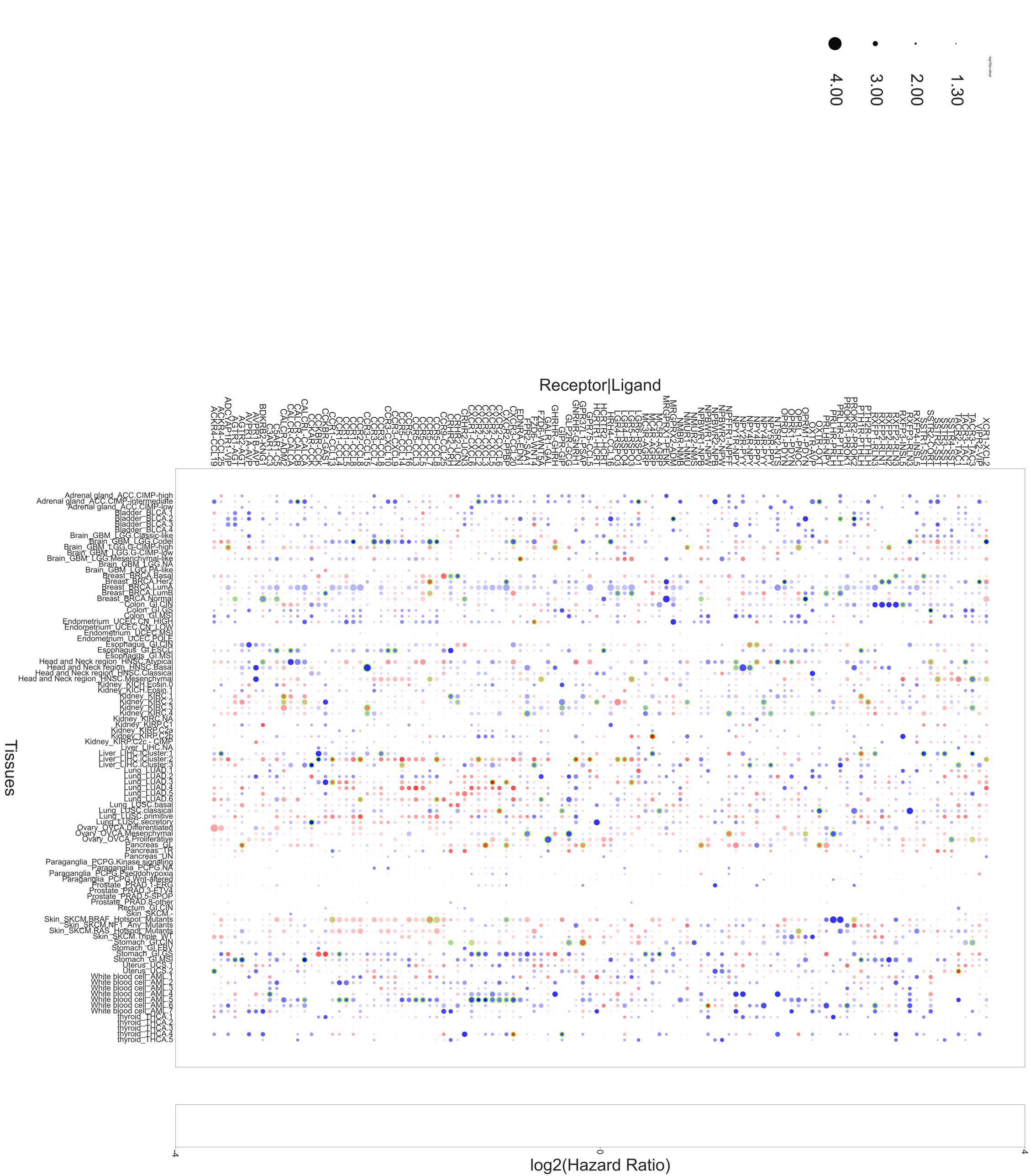
-log10(p-value)
1.30
2.00
3.00
4.00
Receptor|Ligand
XCR1-XCL2
VIPR2-VIP
TACR3-TAC3
TACR3-TAC1
TACR2-TAC1
SSTR4-SST
SSTR3-SST
SSTR2-SST
SSTR2-CORT
SSTR1-SST
RXFP4-INSL5
RXFP3-INSL5
RXFP3-RLN3
RXFP2-RLN3
RXFP2-RLN2
RXFP1-RLN2
RXFP1-RLN1
PTH2R-PTHLH
PTH1R-PTHLH
PROKR2-PROK2
PROKR1-PROK1
PRLHR-PRLH
PRLHR-NPY
OXTR-OXT
OPRM1-PDYN
OPRL1-PNOC
OPRK1-PDYN
OPRD1-PDYN
NTSR2-NTS
NPY5R-PPY
NPY4R-PPY
NPY4R-PPY
NPY2R-PYY
NPY1R-NPY
NPFFR1-NPFF
NPBWR2-NPW
NPBWR2-NPB
NPBWR1-NPW
NPBWR1-NPB
NMUR2-NMS
NMUR1-NMU
NMBR-NMB
MRGPRX2-ADM
MRGPRX1-PENK
MC5R-AGRP
MC4R-AGRP
MC3R-AGRP
LGR6-RSPO1
LGR5-RSPO1
LGR4-RSPO4
LGR4-RSPO3
HRH4-CCL16
HCRTR2-HCRT
HCRTR1-HCRT
GPR37L1-PSAP
GPR75-CCL5
GNRHR-GNRH1
GLP2R-GCG
GLP1R-GCG
GIPR-GIP
GHRHR-GHRH
GALR1-GAL
FZD6-WNT14
FPR2-SAA1
EDNRA-EDN1
CXCR3-CCL20
CXCR2-PPBP
CXCR2-CXCL6
CXCR2-CXCL5
CXCR2-CXCL3
CXCR2-CXCL2
CXCR1-CXCL6
CRHR2-UCN3
CRHR2-UCN
CRHR2-CRH
CCR9-CCL25
CCR5-CCL8
CCR5-CCL7
CCR5-CCL5
CCR5-CCL3
CCR5-CCL16
CCR5-CCL14
CCR3-CXCL9
CCR3-CXCL10
CCR3-CCL8
CCR3-CCL7
CCR3-CCL15
CCR2-CCL8
CCR1-CCL8
CCR1-CCL5
CCR1-CCL4
CCR1-CCL13
CCKBR-CCK
CCKBR-CCK
CALCRL-CALCA
CALCR-CALCA
CALCR-CALCB
CALCR-ADM2
C5AR1-C5
C3AR1-C3
BDKRB2-KNG1
AVPR1B-AVP
AVPR1A-AVP
AGTR2-AGT
AGTR1-AGT
ADCYAP1R1-VIP
ACKR4-CCL25
ACKR4-CCL19
Tissues
Adrenal gland_ACC.CIMP-high
Adrenal gland_ACC.CIMP-intermediate
Adrenal gland_ACC.CIMP-low
Bladder_BLCA.1
Bladder_BLCA.2
Bladder_BLCA.3
Bladder_BLCA.4
Brain_GBM_LGG.Classic-like
Brain_GBM_LGG.Codel
Brain_GBM_LGG.G-CIMP-high
Brain_GBM_LGG.G-CIMP-low
Brain_GBM_LGG.Mesenchymal-like
Brain_GBM_LGG.NA
Brain_GBM_LGG.PA-like
Breast_BRCA.Basal
Breast_BRCA.Her2
Breast_BRCA.LumA
Breast_BRCA.LumB
Breast_BRCA.Normal
Colon_GI.CIN
Colon_GI.GS
Colon_GI.MSI
Endometrium_UCEC.CN_HIGH
Endometrium_UCEC.CN_LOW
Endometrium_UCEC.MSI
Endometrium_UCEC.POLE
Esophagus_GI.CIN
Esophagus_GI.ESCC
Esophagus_GI.MSI
Head and Neck region_HNSC.Atypical
Head and Neck region_HNSC.Basal
Head and Neck region_HNSC.Classical
Head and Neck region_HNSC.Mesenchymal
Kidney_KICH.Eosin.0
Kidney_KICH.Eosin.1
Kidney_KIRC.1
Kidney_KIRC.2
Kidney_KIRC.3
Kidney_KIRC.4
Kidney_KIRC.NA
Kidney_KIRP.C1
Kidney_KIRP.C2a
Kidney_KIRP.C2b
Kidney_KIRP.C2c - CIMP
Liver_LIHC.NA
Liver_LIHC.iCluster:1
Liver_LIHC.iCluster:2
Liver_LIHC.iCluster:3
Lung_LUAD.1
Lung_LUAD.2
Lung_LUAD.3
Lung_LUAD.4
Lung_LUAD.5
Lung_LUAD.6
Lung_LUSC.basal
Lung_LUSC.classical
Lung_LUSC.primitive
Lung_LUSC.secretory
Ovary_OVCA.Differentiated
Ovary_OVCA.Mesenchymal
Ovary_OVCA.Proliferative
Pancreas_GI.
Pancreas_TR
Pancreas_UN
Paraganglia_PCPG.Kinase signaling
Paraganglia_PCPG.NA
Paraganglia_PCPG.Pseudohypoxia
Paraganglia_PCPG.Wnt-altered
Prostate_PRAD.1-ERG
Prostate_PRAD.3-ETV4
Prostate_PRAD.5-SPOP
Prostate_PRAD.8-other
Rectum_GI.CIN
Skin_SKCM.-
Skin_SKCM.BRAF_Hotspot_Mutants
Skin_SKCM.NF1_Any_Mutants
Skin_SKCM.RAS_Hotspot_Mutants
Skin_SKCM.Triple_WT
Stomach_GI.CIN
Stomach_GI.EBV
Stomach_GI.GS
Stomach_GI.MSI
Uterus_UCS.1
Uterus_UCS.2
White blood cell_AML.1
White blood cell_AML.2
White blood cell_AML.3
White blood cell_AML.4
White blood cell_AML.5
White blood cell_AML.6
White blood cell_AML.7
thyroid_THCA.1
thyroid_THCA.2
thyroid_THCA.3
thyroid_THCA.4
thyroid_THCA.5
-4
0
4
log2(Hazard Ratio)

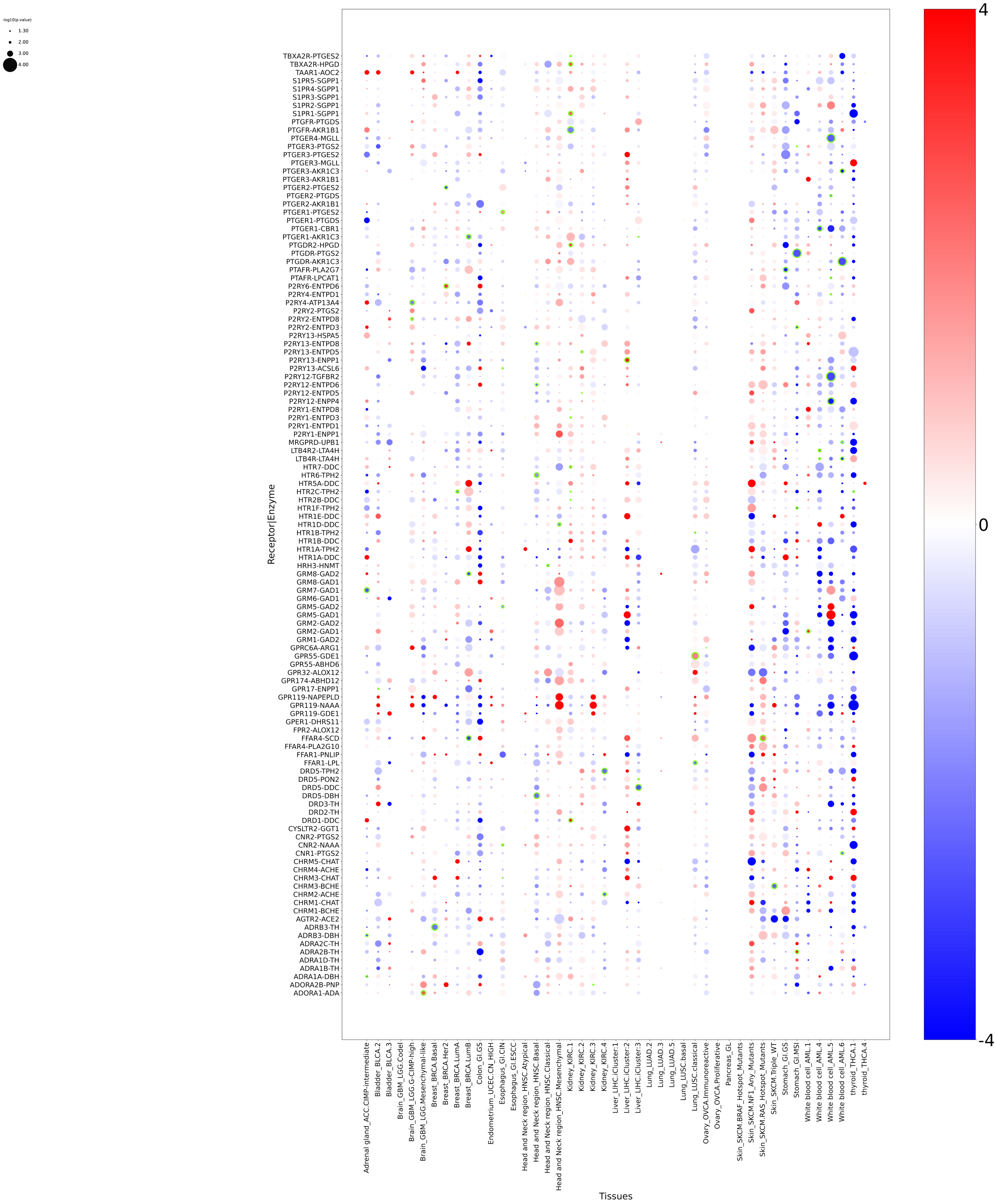
-log10(p-value)
1.30
2.00
3.00
4.00
Receptor|Enzyme
TBXA2R-PTGES2
TBXA2R-HPGD
TAAR1-AOC2
S1PR5-SGPP1
S1PR4-SGPP1
S1PR3-SGPP1
S1PR2-SGPP1
S1PR1-SGPP1
PTGFR-PTGDS
PTGFR-AKR1B1
PTGER4-MGLL
PTGER3-PTGS2
PTGER3-PTGES2
PTGER3-MGLL
PTGER3-AKR1C3
PTGER3-AKR1B1
PTGER2-PTGES2
PTGER2-PTGDS
PTGER2-AKR1B1
PTGER1-PTGES2
PTGER1-PTGDS
PTGER1-CBR1
PTGER1-AKR1C3
PTGDR2-HPGD
PTGDR-PTGS2
PTGDR-AKR1C3
PTAFR-PLA2G7
PTAFR-LPCAT1
P2RY6-ENTPD6
P2RY4-ENTPD1
P2RY4-ATP13A4
P2RY2-PTGS2
P2RY2-ENTPD8
P2RY2-ENTPD3
P2RY13-HSPA5
P2RY13-ENTPD8
P2RY13-ENTPD5
P2RY13-ENPP1
P2RY13-ACSL6
P2RY12-TGFBR2
P2RY12-ENTPD6
P2RY12-ENTPD5
P2RY12-ENPP4
P2RY1-ENTPD8
P2RY1-ENTPD3
P2RY1-ENTPD1
P2RY1-ENPP1
MRGPRD-UPB1
LTB4R2-LTA4H
LTB4R-LTA4H
HTR7-DDC
HTR6-TPH2
HTR5A-DDC
HTR2C-TPH2
HTR2B-DDC
HTR1F-TPH2
HTR1E-DDC
HTR1D-DDC
HTR1B-TPH2
HTR1B-DDC
HTR1A-TPH2
HTR1A-DDC
HRH3-HNMT
GRM8-GAD2
GRM8-GAD1
GRM7-GAD1
GRM6-GAD1
GRM5-GAD2
GRM5-GAD1
GRM2-GAD2
GRM2-GAD1
GRM1-GAD2
GPRC6A-ARG1
GPR55-GDE1
GPR55-ABHD6
GPR32-ALOX12
GPR174-ABHD12
GPR17-ENPP1
GPR119-NAPEPLD
GPR119-NAAA
GPR119-GDE1
GPER1-DHRS11
FPR2-ALOX12
FFAR4-SCD
FFAR4-PLA2G10
FFAR1-PNLIP
FFAR1-LPL
DRD5-TPH2
DRD5-PON2
DRD5-DDC
DRD5-DBH
DRD3-TH
DRD2-TH
DRD1-DDC
CYSLTR2-GGT1
CNR2-PTGS2
CNR2-NAAA
CNR1-PTGS2
CHRM5-CHAT
CHRM4-ACHE
CHRM3-CHAT
CHRM3-BCHE
CHRM2-ACHE
CHRM1-CHAT
CHRM1-BCHE
AGTR2-ACE2
ADRB3-TH
ADRB3-DBH
ADRA2C-TH
ADRA2B-TH
ADRA1D-TH
ADRA1B-TH
ADRA1A-DBH
ADORA2B-PNP
ADORA1-ADA
Adrenal gland_ACC.CIMP-intermediate
Bladder_BLCA.2
Bladder_BLCA.3
Brain_GBM_LGG.Codel
Brain_GBM_LGG.G-CIMP-high
Brain_GBM_LGG.Mesenchymal-like
Breast_BRCA.Basal
Breast_BRCA.Her2
Breast_BRCA.LumA
Breast_BRCA.LumB
Colon_GI.GS
Endometrium_UCEC.CN_HIGH
Esophagus_GI.CIN
Esophagus_GI.ESCC
Head and Neck region_HNSC.Atypical
Head and Neck region_HNSC.Basal
Head and Neck region_HNSC.Classical
Head and Neck region_HNSC.Mesenchymal
Kidney_KIRC.1
Kidney_KIRC.2
Kidney_KIRC.3
Kidney_KIRC.4
Liver_LIHC.iCluster:1
Liver_LIHC.iCluster:2
Liver_LIHC.iCluster:3
Lung_LUAD.2
Lung_LUAD.3
Lung_LUAD.5
Lung_LUSC.basal
Lung_LUSC.classical
Ovary_OVCA.Immunoreactive
Ovary_OVCA.Proliferative
Pancreas_GL
Skin_SKCM.BRAF_Hotspot_Mutants
Skin_SKCM.NF1_Any_Mutants
Skin_SKCM.RAS_Hotspot_Mutants
Skin_SKCM.Triple_WT
Stomach_GI.GS
Stomach_GI.MSI
White blood cell_AML.1
White blood cell_AML.4
White blood cell_AML.5
White blood cell_AML.6
thyroid_THCA.1
thyroid_THCA.4
Tissues
4
0
-4
log2(HR)

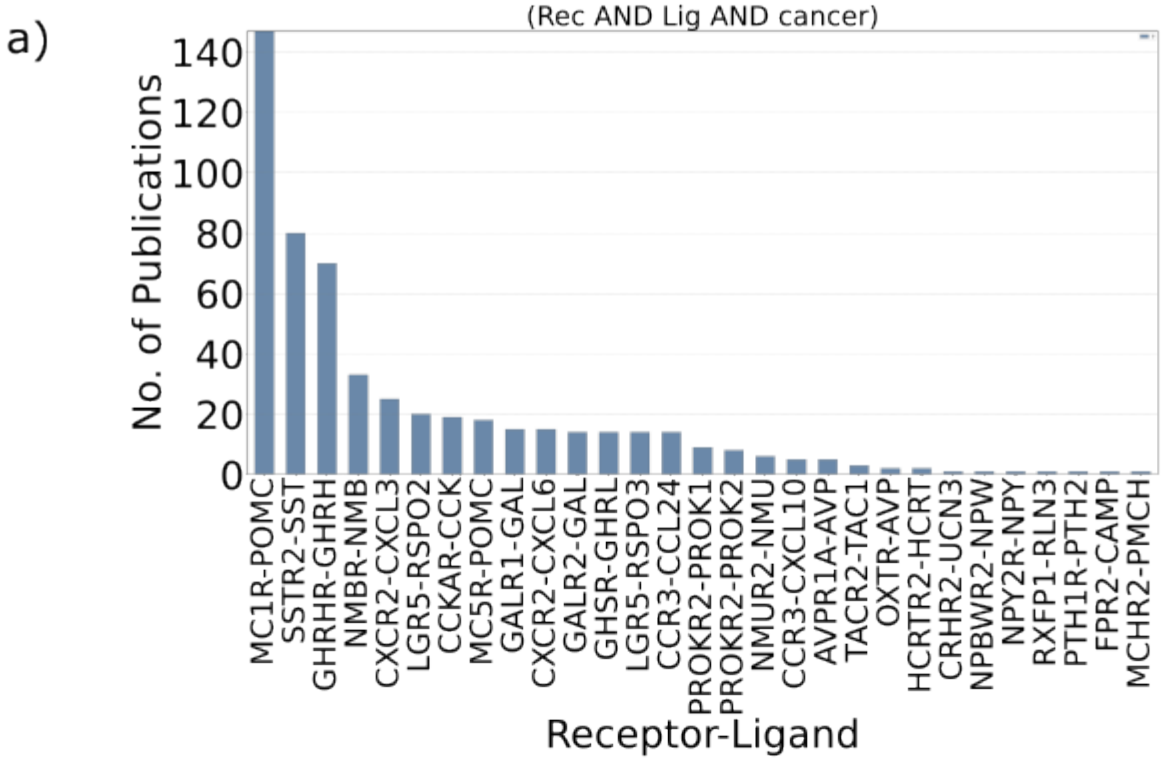
a)
(Rec AND Lig AND cancer)
No. of Publications
0
20
40
60
80
100
120
140
MC1R-POMC
SSTR2-SST
GHRHR-GHRH
NMBR-NMB
CXCR2-CXCL3
LGR5-RSPO2
CCKAR-CCK
MC5R-POMC
GALR1-GAL
CXCR2-CXCL6
GALR2-GAL
GHSR-GHRL
LGR5-RSPO3
CCR3-CCL24
PROKR2-PROK1
PROKR2-PROK2
NMUR2-NMU
CCR3-CXCL10
AVPR1A-AVP
TACR2-TAC1
OXTR-AVP
HCRTR2-HCRT
CRHR2-UCN3
NPBWR2-NPW
NPY2R-NPY
RXFP1-RLN3
PTH1R-PTH2
FPR2-CAMP
MCHR2-PMCH
Receptor-Ligand

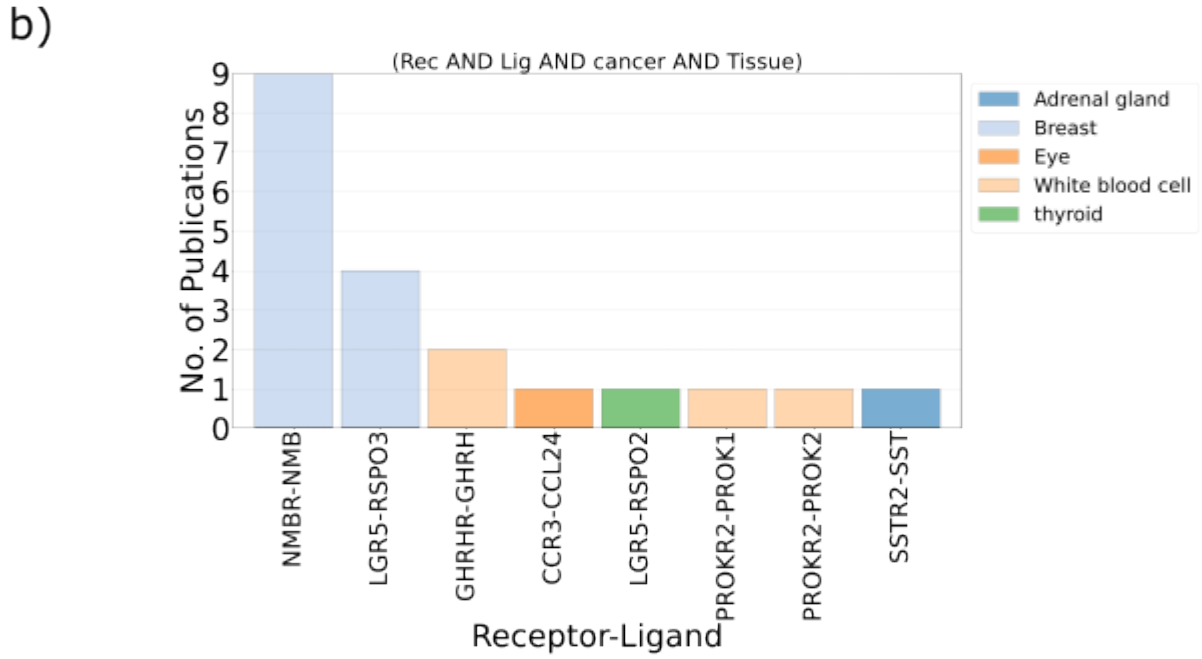
b)
(Rec AND Lig AND cancer AND Tissue)
No. of Publications
0
1
2
3
4
5
6
7
8
9
Adrenal gland
Breast
Eye
White blood cell
thyroid
NMBR-NMB
LGR5-RSPO3
GHRHR-GHRH
CCR3-CCL24
LGR5-RSPO2
PROKR2-PROK1
PROKR2-PROK2
SSTR2-SST
Receptor-Ligand

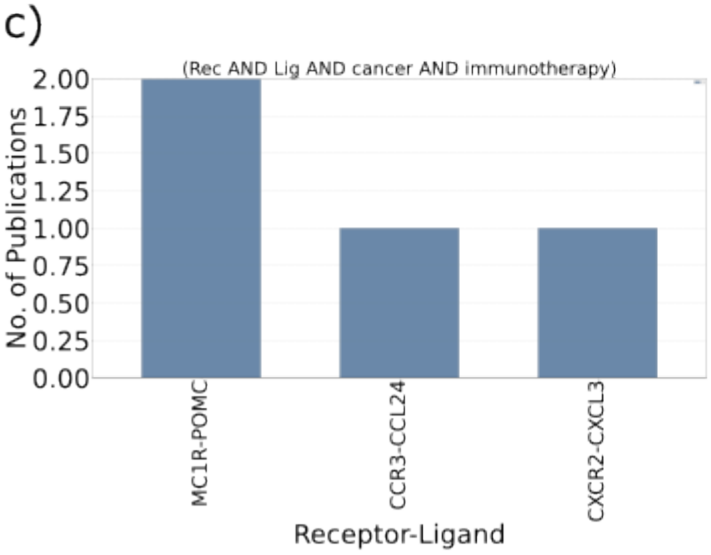
c)
(Rec AND Lig AND cancer AND immunotherapy)
No. of Publications
0.00
0.25
0.50
0.75
1.00
1.25
1.50
1.75
2.00
MC1R-POMC
CCR3-CCL24
CXCR2-CXCL3
Receptor-Ligand

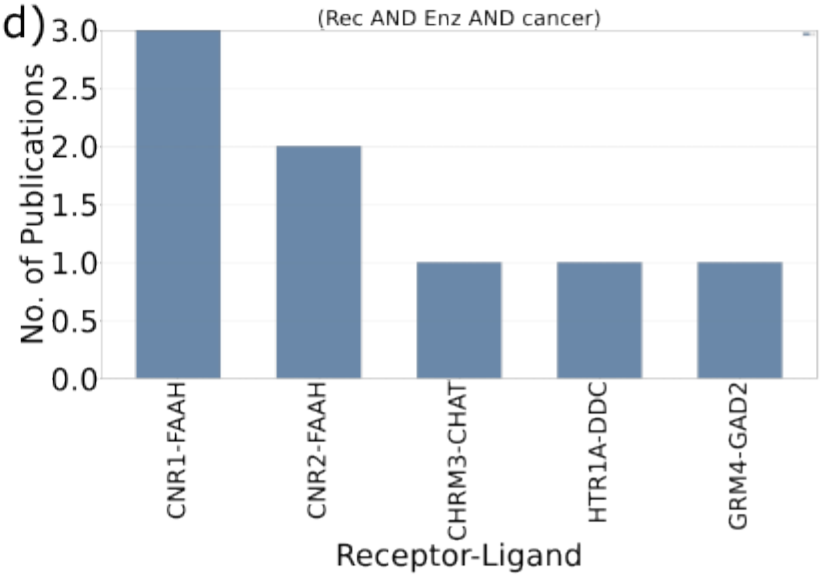
d)
(Rec AND Enz AND cancer)
No. of Publications
0.0
0.5
1.0
1.5
2.0
2.5
3.0
CNR1-FAAH
CNR2-FAAH
CHRM3-CHAT
HTR1A-DDC
GRM4-GAD2
Receptor-Ligand